Adaptor protein complex interaction map in Arabidopsis identifies P34 as a common stability regulator

Nature Plants

Wang, Peng; Siao, Wei; Zhao, Xiuyang; Arora, Deepanksha; Wang, Ren et al

https://doi.org/10.1038/s41477-022-01328-2

This publication is made publicly available in the institutional repository of Wageningen University and Research, under the terms of article 25fa of the Dutch Copyright Act, also known as the Amendment Taverne.

Article 25fa states that the author of a short scientific work funded either wholly or partially by Dutch public funds is entitled to make that work publicly available for no consideration following a reasonable period of time after the work was first published, provided that clear reference is made to the source of the first publication of the work.

This publication is distributed using the principles as determined in the Association of Universities in the Netherlands (VSNU) 'Article 25fa implementation' project. According to these principles research outputs of researchers employed by Dutch Universities that comply with the legal requirements of Article 25fa of the Dutch Copyright Act are distributed online and free of cost or other barriers in institutional repositories. Research outputs are distributed six months after their first online publication in the original published version and with proper attribution to the source of the original publication.

You are permitted to download and use the publication for personal purposes. All rights remain with the author(s) and / or copyright owner(s) of this work. Any use of the publication or parts of it other than authorised under article 25fa of the Dutch Copyright act is prohibited. Wageningen University & Research and the author(s) of this publication shall not be held responsible or liable for any damages resulting from your (re)use of this publication.

For questions regarding the public availability of this publication please contact openaccess.library@wur.nl

nature plants

Article

https://doi.org/10.1038/s41477-022-01328-2

Adaptor protein complex interaction map in *Arabidopsis* identifies P34 as a common stability regulator

Received: 21 June 2022

Accepted: 5 December 2022

Published online: 12 January 2023

Check for updates

Peng Wang[1,2,9], Wei Siao[1,2,9,10] ✉, Xiuyang Zhao[1,2], Deepanksha Arora[1,2], Ren Wang[1,2], Dominique Eeckhout[1,2], Jelle Van Leene[1,2], Rahul Kumar[1,2,7], Anaxi Houbaert[1,2,8], Nancy De Winne[1,2], Evelien Mylle[1,2], Michael Vandorpe[1,2], Ruud A. Korver[3], Christa Testerink[3,4], Kris Gevaert[5,6], Steffen Vanneste[1,2], Geert De Jaeger[1,2], Daniël Van Damme[1,2] & Eugenia Russinova[1,2,10] ✉

Adaptor protein (AP) complexes are evolutionarily conserved vesicle transport regulators that recruit coat proteins, membrane cargoes and coated vesicle accessory proteins. As in plants endocytic and post-Golgi trafficking intersect at the *trans*-Golgi network, unique mechanisms for sorting cargoes of overlapping vesicular routes are anticipated. The plant AP complexes are part of the sorting machinery, but despite some functional information, their cargoes, accessory proteins and regulation remain largely unknown. Here, by means of various proteomics approaches, we generated the overall interactome of the five AP and the TPLATE complexes in *Arabidopsis thaliana*. The interactome converged on a number of hub proteins, including the thus far unknown adaptin binding-like protein, designated P34. P34 interacted with the clathrin-associated AP complexes, controlled their stability and, subsequently, influenced clathrin-mediated endocytosis and various post-Golgi trafficking routes. Altogether, the AP interactome network offers substantial resources for further discoveries of unknown endomembrane trafficking regulators in plant cells.

The transport of integral membrane proteins from one compartment to another subcellular destination within the endomembrane system is essential for all living eukaryotic cells. This transport is mostly mediated by coated vesicles that are formed by the recruitment of coat proteins onto a particular membrane compartment where they bind adaptors, and other accessory molecules to promote membrane curvature and collect the vesicle cargo[1]. Critical for this process is the fine-tuned control of intracellular cargo sorting, which relies on signals within the cargo proteins and on the specific adaptor protein (AP) complexes-mediated cargo recognition. Five AP complexes, designated AP-1 to AP-5, each involved in a distinct vesicle trafficking pathway, have been identified in higher eukaryotes[2]. The five AP complexes are heterotetrameric proteins that contain two large subunits (β1 to β5 and γ, α, δ, ε and ζ), a medium subunit (μ1 to μ5) and a small subunit

[1]Department of Plant Biotechnology and Bioinformatics, Ghent University, Ghent, Belgium. [2]Center for Plant Systems Biology, VIB, Ghent, Belgium. [3]Plant Physiology and Cell Biology, Swammerdam Institute for Life Sciences, University of Amsterdam, Amsterdam, the Netherlands. [4]Laboratory of Plant Physiology, Wageningen University & Research, Wageningen, the Netherlands. [5]Department of Biomolecular Medicine, Ghent University, Ghent, Belgium. [6]Center for Medical Biotechnology, VIB, Ghent, Belgium. [7]Present address: Department of Plant Sciences, University of Hyderabad, Hyderabad, India. [8]Present address: Department of Plant Molecular Biology, University of Lausanne, Lausanne, Switzerland. [9]These authors contributed equally: Peng Wang, Wei Siao. [10]These authors jointly supervised this work: Wei Siao, Eugenia Russinova. ✉e-mail: wei.siao@psb.vib-ugent.be; eurus@psb.vib-ugent.be

(σ1 to σ5)[3]. Whereas in mammalian cells AP-1, AP-2 and AP-3 operate in concert with the scaffolding molecule clathrin to generate clathrin-coated vesicles (CCVs), AP-4 and AP-5 function independently of clathrin[3].

In plant cells, the major membrane trafficking pathways, including secretory, endocytic and vacuolar pathways, intersect at the *trans*-Golgi network (TGN)/early endosome (EE)[4]. Over the past decade, some functions of AP-1 to AP-4 have been characterized in the model plant *Arabidopsis thaliana*[5]. Although sequence-based homology searches have predicted a partial AP-5 in plant genomes[2], the AP-5 function and composition remain undetermined[6]. Plant AP-1 associates with TGN/EE and transports cargoes to the plasma membrane (PM), cell plates or vacuoles, and loss of the AP-1 function leads to impeded growth, cytokinesis defects and male and female sterility[7–10]. Plant AP-2 facilitates clathrin-mediated endocytosis (CME) of various PM proteins, such as the PIN-FORMED[11] proteins, BR INSENSITIVE1 (BRI1)[12–14] receptor and the boron transporter REQUIRES HIGH BORON1 (BOR1), and is important for reproductive organ development[15,16]. AP-3 enables the vacuolar targeting of the SUCROSE TRANSPORTER4 (SUC4) and the R-SNARE subfamily members VAMP713, and AP-3 function loss reduces germination and affects gravitropic responses[17–20]. AP-4 mediates vacuolar protein sorting and the recruitment of the ENTH domain protein MODIFIED TRANSPORT TO THE VACUOLE1 (MTV1) at the TGN/EE, and AP-4 deficiency causes growth defects and suppresses hypersensitive cell death upon infection with avirulent bacteria[21–24]. Alongside AP-2, an ancient heterooctameric adaptor complex, designated the TPLATE complex (TPC), is also required for CME at the PM in plant cells[25,26]. Knockout of single subunits of TPC caused male sterility, whereas silencing triggered seedling lethality[25,27] and abolished the endocytic flux, as also observed upon conditional inactivation of the complex[28].

In addition to the coat proteins and the tetrameric AP complexes, CME in mammalian and yeast cells requires the activity of more than 60 endocytic accessory proteins (EAPs) that function as scaffolds, cargo recruiters, membrane curvature generators and sensors, as well as CME regulators[29,30]. Such EAPs have been found either by comparative proteomics of CCVs[31,32] or by affinity purification coupled to mass spectrometry (AP–MS) as binding partners of the C-terminal appendages or EAR domains of the large subunits of AP complexes[33,34]. Although some EAPs have been identified on the basis of sequence homology[4,6] and recently by proteomic analysis of *Arabidopsis* CCVs[35], their involvement in vesicle formation in plant cells remains largely uncharacterized.

In this Article, using AP–MS and proximity labelling (PL) coupled to MS (PL–MS), we generated a comprehensive interactome of the six AP complexes in *Arabidopsis*, thereby providing informative resources and links between vesicle transports and their regulators. We identified the AP-5 complex and its associated core subunits, spatacsin (SPG11) and spastizin (SPG15 also known as ZFYVE26), in *Arabidopsis* cells. The interactomes of the clathrin-associated AP complexes in *Arabidopsis*, AP-1, AP-2 and AP-4 (ref. 35), converged on several hub proteins, of which the adaptin binding-like protein, designated P34, was functionally characterized. The *P34* gene is essential for *Arabidopsis* because a loss-of-function mutation led to embryogenesis defects. We show that P34 controls the stability of AP-1, AP-2 and AP-4, but not of AP-3, and, as such, influences CME and various post-Golgi trafficking routes.

Results

The AP interactome reveals two interconnected networks

To gain further insight into the function of the five AP complexes and TPC in plants, we performed a targeted interaction screen in *Arabidopsis* cell suspension cultures (PSB-D). To this end, we applied a series of tandem affinity purification (TAP), single-step AP–MS and PL–MS experiments (for more details, see Methods). Previously, these interactome analyses had successfully been used for the identification of the core AP-2 and TPC in *Arabidopsis*[12,25,36]. Upon integrating all interactome analyses including further network extension through a selection of reciprocal (T)AP–MS experiments (see below), we generated a comprehensive network of 926 interactions among 536 proteins (Fig. 1 and Supplementary Table 1).

First, we analysed AP-1 and AP-2 using AP1G1, AP1G2, AP1S1, AP1/2B1, AP2A1 and AP2S as baits for TAP–MS, retrieving 110 interactions among 52 proteins (Fig. 1a and Supplementary Table 1). As a complementary approach, we mapped proximal interactors of the AP-2 and the TPC with PL using AP2M and the TPC subunit TML as bait proteins fused to the biotin ligase TurboID tag, revealing 419 interactions among 344 proteins (Fig. 1a and Supplementary Table 1). Both the TAP and PL approaches were successful, because all the core subunits of AP-1, AP-2 and TPC (except for the smaller LOLITA protein) were identified (Fig. 1b and Extended Data Fig. 1). Consistent with the fact that AP-2 functions in endocytosis and shares the β subunit with AP-1, AP-2 associated with both AP-1 and TPC (Fig. 2), because AP1M2, AP1S1 and all TPC subunits, except for the LOLITA, were found with AP-2 subunits as baits (Fig. 2, right inset). When the AP-1 subunits were used as baits, all AP-2 subunits, except AP2A1, were identified in these experiments, demonstrating the interconnection between AP-1 and AP-2. Besides the core AP-1, AP-2 and TPC subunits, several known accessory proteins linked to endocytosis and vesicle trafficking were detected through PL, such as the clathrin light chain subunit 2 (CLC2), four dynamin-related proteins (DRP1A, DRP1E, DRP2A and DRP2B), the clathrin uncoating factors AUXILIN-LIKE1 and AUXILIN-LIKE4 (ref. 37), the R-SNARE protein VESICLE-ASSOCIATED MEMBRANE PROTEIN 721 (VAMP721)[38,39] and six ENTH/ANTH/VHS accessory proteins (ECA4, PICALM3, EPSIN2, EPSIN3, TOL6 and TOL9) Their specific PL identification concurs with the fact that PL enhances the detection of membrane-related protein interactions, when compared with protein complex analysis by (T)AP–MS[36]. Nonetheless, the TAP–MS analysis on the core AP-1, AP-2 and TPC subunits retrieved also additional proteins that can be linked to endocytosis, as witnessed by the co-purification of an *Arabidopsis* homologue (AT3G58600) of the human ADAPTIN EAR-BINDING COAT-ASSOCIATED PROTEIN-1 (NECAP-1)[40] with three AP-1 subunits in TAP–MS. The interaction between NECAP-1 and AP-1 was confirmed in reciprocal TAP–MS experiments with NECAP-1 as bait, in which all AP-1 subunits but none of the AP-2 subunits were detected (Fig. 1b and Supplementary Table 1).

These TAP and PL analyses clearly demonstrate the robustness of the interactome data, not only providing valuable insight into the functioning of the core AP-1, AP-2 and TPC, but potentially also revealing unknown accessory proteins. Notably, three proteins with previously undetermined functions in plant endomembrane trafficking, a GTP-binding protein (AT5G65960), a protein kinase superfamily protein (AT2G32850) and the BCL-2-ASSOCIATED ATHANOGENE4 (BAG4) protein[41] (AT3G51780), were identified with multiple AP-2 subunits and TML as bait proteins, highlighting them as novel candidate accessory proteins. Sequence homology analysis revealed that the GTP-binding protein is a putative plant homologue of the human α- and γ-adaptin binding protein (AAGAB) P34 (refs. 42, 43), with 23% identity and 38% similarity (Extended Data Fig. 2), whereas the uncharacterized protein kinase is a plant homologue of the human AP2-ASSOCIATED PROTEIN KINASE1 (AAK1)[44,45] with 43% identity and 62% similarity (Extended Data Fig. 3). The BAG family protein BAG4 is a member of an evolutionarily conserved group of co-chaperones found in yeasts, animals and plants, linked mainly to apoptosis[41]. To further consolidate the predicted role of P34, BAG4 and AAK1 in plant vesicle trafficking based on sequence similarity to their mammalian orthologues[41,42,45], reciprocal TAP–MS analyses using these three proteins as baits identified 87 interactions among 73 proteins (Fig. 1 and Supplementary Table 1). The reciprocal TAP–MS analyses indicated that, also in plants, P34, AAK1 and BAG4 are linked with vesicle trafficking, because numerous AP-1, AP-2, AP-4 and TPC subunits, clathrin and ENTH/ANTH/VHS proteins were retrieved. The TAP–MS experiments with AAK1 confirmed its interaction with AP-2 and clathrin heavy chains (CHCs). Intriguingly, highly stable and

https://doi.org/10.1038/s41477-022-01328-2

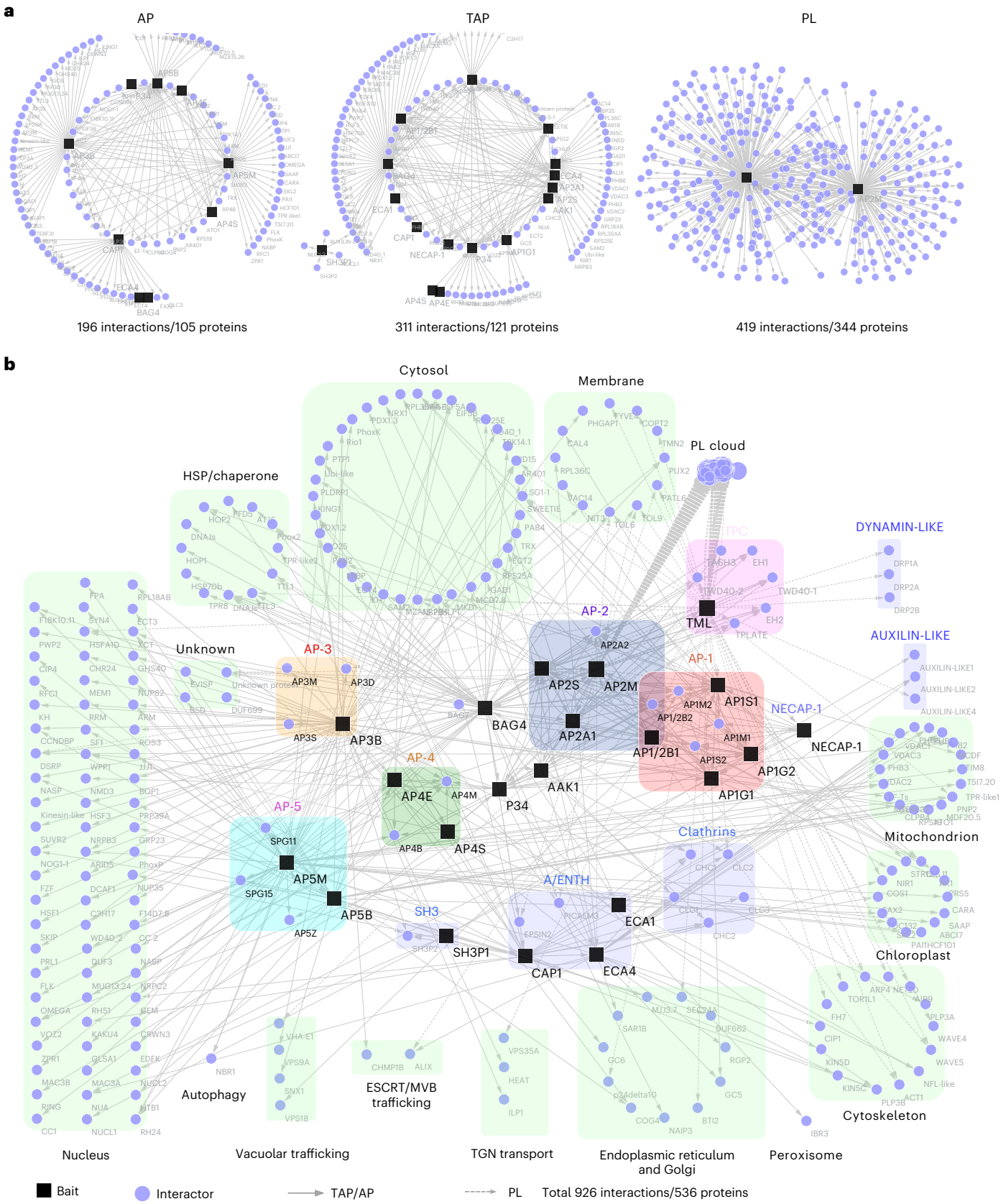

Fig. 1 | Integrative interaction network of six multimeric adaptor complexes and their accessory proteins. a, Thirteen proteins (AP1G1, AP1G2, AP1S1, AP2A1, AP2B1, AP2S, BAG4, P34, AAK1, NECAP-1, AtECA1, AtECA4 and SH3P1) were used as baits for TAP–MS, six proteins (AP3B, AP4E, AP4S, AP5B, AP5M and CAP1) for AP–MS and two proteins (AP2M and TML) for PL–MS. **b**, Visualization of the protein interactions. Rounded rectangles in different colours represent the components of different complexes, including AP-1 (red), AP-2 (blue), AP-3 (orange), AP-4 (green), AP-5 (cyan), TPC (magenta) and other accessory proteins (light purple). The PL cloud indicates a group of proteins identified by PL–MS without direct link to vesicle trafficking. The proteins co-purified with the baits are annotated by their known or predicted subcellular localizations or trafficking pathways as indicated (light green rectangles). AP, affinity purification.

https://doi.org/10.1038/s41477-022-01328-2

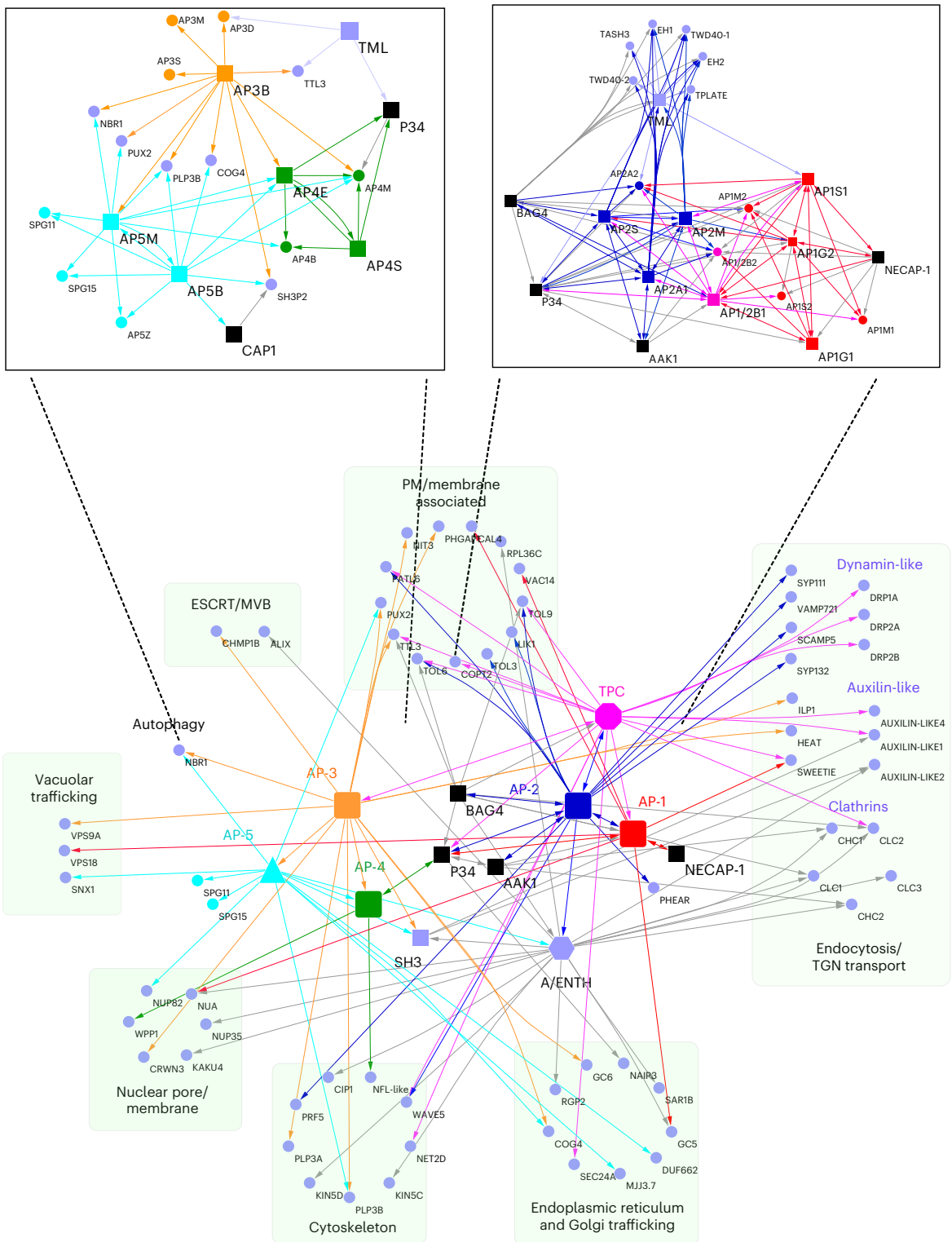

Fig. 2 | Selection from the AP interactome of putative regulators and their crosstalk in vesicle trafficking. Interactors related to membrane and protein transport were selected. The subunits of each AP complex are combined and shown as individual units (nodes) in colours (AP-1, red; AP-2, blue; AP-3, orange; AP-4, green; AP-5, cyan; TPC, magenta). The purple hexagon and square nodes represent the protein members of A/ENTH and SH3, respectively. P34, BAG4 and AAK1 proteins are shown in black squares. The purple round nodes are the interactors that are functionally linked with protein transport. Source and target nodes of the arrows indicate the baits and the targets, respectively. Insets: detailed interaction networks of the individual subunits of AP-3, AP-4 and AP-5 (left) and of AP-1, AP-2 and TPC (right).

stoichiometric interactions were found between P34 and multiple AP-2 and AP-1 subunits, while interacting with the AP-4 subunit AP4M as well, although this interaction was less prevalent. Also with BAG4, multiple members of both the AP-2 and AP-1 were co-purified, in addition to five subunits of the TPC, two CLCs and multiple ENTH/ANTH/VHS proteins. To further extend our endocytosis-related network, the three AP180-amino-terminal-homology (ANTH)-domain-containing proteins ECA1, ECA4 and CAP1, which were isolated with BAG4 as a bait

https://doi.org/10.1038/s41477-022-01328-2

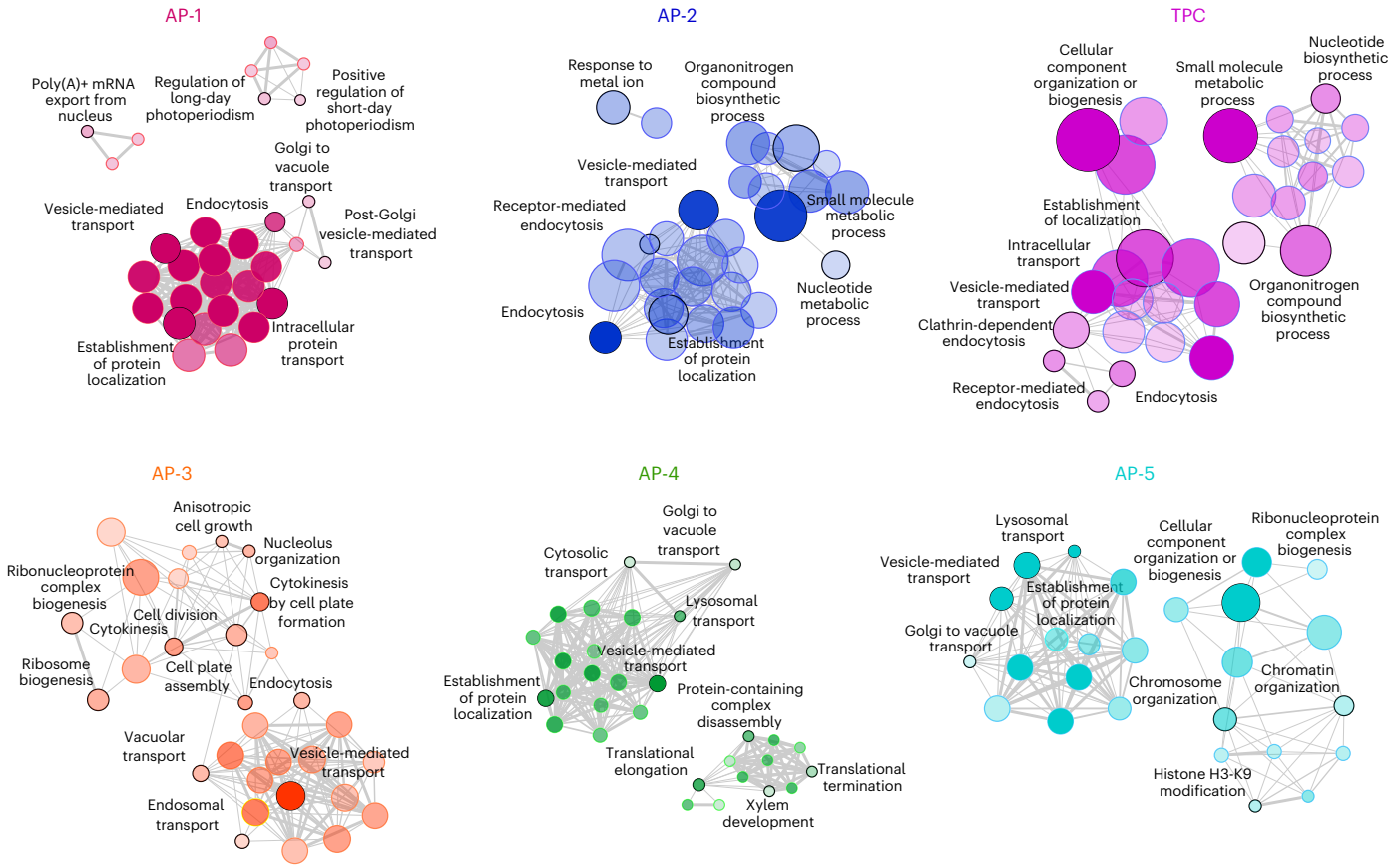

Fig. 3 | GO term enrichment analysis of the AP-associated proteins. Hierarchical clustering trees show the enriched gene sets associated with different AP complexes and accessory proteins. Each node indicates a significantly enriched GO term (FDR <0.05). The size and colour of the node represent the number of genes in the gene set and different complexes, respectively. The colour hue corresponds to the proportion of each cluster associated with the term. Two terms (nodes) are connected, when they share 20% or more genes. The line thickness indicates the number of shared genes between two terms. Selected GO terms (outlined circles) are annotated.

and are involved in membrane budding processes[39], were selected for reciprocal TAP–MS (ECA1 and ECA4) or AP–MS (CAP1). These analyses support that the ECA4 and CAP1 functions are associated with CCVs, as CLCs and CHCs were isolated with these baits. Moreover, ECA4 and CAP1 seem to act in one protein complex, because both proteins were abundantly co-purified which each other. Similarly, also P34, AAK1 and BAG4 were isolated with each other. Therefore, our interactome analyses imply that AP-1, AP-2 and TPC are intrinsically connected to each other, and that P34, BAG4 and AAK1 function as accessory proteins that link these complexes.

Next, we built the interactome network of AP-3 and AP-4 by means of their large subunits AP3B and AP4E and the small AP-4 subunit (AP4S) as baits for single-step AP–MS. The resulting AP-3 and AP-4 network consisted of 77 interactions among 54 proteins, demonstrating that, in addition to the interactions between core subunits within each complex, AP-3, AP-4 and AP-5 were linked with each other (Fig. 2), because AP4E, AP4M and AP5M were identified with AP3B as bait (Fig. 2, left inset). Markedly, P34 was also detected with both AP-4 subunits, in agreement with the identification of the AP4M subunit in the TAP–MS with P34 as bait.

Identification of the *Arabidopsis* AP-5 complex

Although sequence homology searches have identified three putative genes encoding AP-5 subunits in *Arabidopsis*, *AP5B* (AT3G19870), *AP5Z* (AT3G15160) and *AP5M* (AT2G20790)[2], it is still unclear whether they function together as a bona fide complex in plant cells. To discover the core complex and the accessory proteins of AP-5, we used AP5B and AP5M as baits for single-step AP–MS. In total, 102 interactions among 59 proteins were present in the AP-5 network (Fig. 1 and Supplementary Table 1) and all three AP-5 subunits were identified together with the thus far uncharacterized proteins in plants ZINC FINGER FYVE DOMAIN-CONTAINING PROTEIN (ZFYVE) (AT2G25730) and SPATACSIN CARBOXY-TERMINUS PROTEIN (AT4G39420). Further sequence alignments revealed the homology of the SPATACSIN CARBOXY-TERMINUS PROTEIN and the ZFYVE protein to the mammalian SPG11 (with 60% similarity and 22.83% identity) and SPG15 (with 49% similarity and 22.57% identity) proteins, respectively, the two known accessory proteins of the AP-5 complex in mammalian cells[2,46]. Consistent with the AP-4 interactome analyses, AP5M co-purified with three AP-4 subunits (Fig. 2, left inset). Taken together, these findings imply that, besides the subclustering of the AP-1, AP-2 and TPC, there is a crosstalk between the vesicle trafficking pathways regulated by AP-5, AP-3 and AP-4. Indeed, the accessory AP SH3P2 was detected using AP3B, AP5B and CAP1 as baits. Interestingly, SH3P2 was also found by means of TAP–MS with its homologue SH3P1 as bait, despite previous reports that SH3P1 and SH3P2 function in different trafficking pathways[47,48].

Functional diversity of the AP complexes in *Arabidopsis*

To gain insight into the function of the AP-complex-interacting partners, we analysed the Gene Ontology (GO) enrichment. All identified proteins were enriched in GO terms linked to protein transport and molecule metabolic process (Fig. 3 and Supplementary Table 2), including 'vesicle-mediated transport' and 'establishment of protein localization'. The GO analysis of an individual AP complex revealed that the proteins

associated with AP-1, AP-2, AP-3 and TPC were present in 'endocytosis', whereas those of AP-4 and AP-5 were enriched in 'lysosomal transport'. The proteins concomitant with the accessory proteins P34, BAG4, AAK1, ECA1, ECA4 and CAP1 were paired with the terms 'CME' and 'clathrin coat assembly'. Additionally, the GO term 'Golgi to vacuole transport' was shared by the AP-1, AP-4 and AP-5 interactors, and the term 'vacuolar transport' was associated with AP-3. Interestingly, specific AP complexes were coupled with some GO terms without direct links to vesicle trafficking. For example, some AP-1 interactors were connected with the terms 'photoperiodism' and 'mRNA export'. AP-2 and TPC shared the GO terms related to metabolic processes, whereas the term 'response to metal ion' occurred only in AP-2. Specifically, AP-3 interactors were enriched in 'cytokinesis' and 'ribosome biogenesis'. By contrast, a cluster of terms related to 'translation', 'protein complex disassembly' and 'xylem development' were associated with the AP-4 interactome. Proteins co-purifying with AP-5 were enriched, on the one side, in 'lysosomal transport' and 'Golgi to vacuole transport' and, on the other side, in 'chromosome organization' and 'histone modifications'. Altogether, the GO analysis revealed putative roles of AP complexes in different physiological pathways, seemingly not connected to endomembrane functions.

Validation of the AP interactomes

As AP-5 had not been characterized in plants, we validated the interactions between the AP-5 subunits with co-immunoprecipitation (co-IP) and ratiometric bimolecular fluorescence complementation (rBiFC) (Fig. 4a–c, Extended Data Fig. 4a and Supplementary Table 3). As predicted, AP5B and AP5M reciprocally co-immunoprecipitated when transiently co-expressed in tobacco (*Nicotiana benthamiana*) leaves (Fig. 4a). Similarly, AP5M co-immunoprecipitated with SPG11 and SPG15, whereas AP5B co-immunoprecipitated with SPG15 (Fig. 4a). In the rBiFC assay, co-expression of AP5M-nYFP (nYFP, the N-terminal fragments of YFP) with AP5B-cYFP (cYFP, the C-terminal fragments of YFP) and AP5Z-nYFP with AP5M-cYFP, but not with AP5B-cYFP, or AP3B-nYFP with AP5M-cYFP, resulted in fluorescence recovery in tobacco epidermal cells (Fig. 4b and Extended Data Fig. 4a). These data confirmed the interactions between AP-5 subunits and SPG proteins, supporting that AP-5 functions as a complex with SPG11 and SPG15 (Fig. 4c) in plant cells, similarly as in mammalian cells[46].

Interactions between the accessory proteins AAK1, BAG4 and P34 and the AP subunits were also validated by co-IP using transgenic *Arabidopsis* plants expressing *p35S:AAK1-GFP*, *p35S:BAG4-GFP*, *p35S:P34-GFP* and *p35S:GFP* constructs and by rBiFC in tobacco leaf epidermal cells (Fig. 4d–l, Extended Data Figs. 4b,c and 5 and Supplementary Table 3). AAK1 co-immunoprecipitated with subunits of AP-1 and AP-2 but not with TPLATE and CHC (Fig. 4d). In the rBiFC assay, co-expression of AAK1-cYFP with AP2A1-nYFP, nYFP-AP2M, nYFP-AP2S or nYFP-AP1/2B1 resulted in fluorescence signals (Fig. 4e and Extended Data Fig. 4b). As AAK1 most likely interacted directly with AP-2 (Fig. 4f), the recovery of the AP1G subunit in the co-IP of AAK1-GFP might result from the interaction with the shared AP1/2B1 subunit. Subsequently, co-IP experiments in *Arabidopsis* and rBiFC confirmed that BAG4 is a hub protein associated with AP-1, AP-2 and TPC (Fig. 4g–i and Extended Data Fig. 4c), whereas P34 interacted with subunits of AP-1, AP-2 and AP-4 (Fig. 4j–l and Extended Data Fig. 5a,f). Interestingly, in the rBiFC assays, P34 also interacted with AP3D and AP5Z subunits (Extended Data Fig. 5b,c), suggesting that P34 binds to various AP complexes in rBiFC (Fig. 4l). However, co-IP in tobacco did not identify an association between P34 and AP3B (Extended Data Fig. 5f). We also checked whether a mutation in one AP complex would affect the interaction between P34 and another AP complex. Subsequent co-IP uncovered that P34 was still associated with AP1G and AP2A in the *ap4m-2* mutant (Extended Data Fig. 5g). Furthermore, interactions between P34, BAG4 and AAK1 were also observed in rBiFC (Extended Data Fig. 5d,e). Interestingly, even though the *Arabidopsis* NECAP-1 was identified in the TAP–MS experiments with AP-1, rBiFC analysis showed an interaction with subunits of both the AP-1 and AP-2 complexes (Extended Data Fig. 6a–c), similarly to NECAP-1 in mammals[40]. The PL analysis with AP2M revealed several unknown PM-associated putative endocytic cargoes, and rBiFC (Extended Data Fig. 6d,e) confirmed the interactions between AP2M and the cytokinesis-specific syntaxin KNOLLE[49] and the FORMIN-LIKE6 (FH6) protein[50]. Collectively, we generated a highly reliable AP interaction network, including the composition of the AP-5, several AP complex accessory proteins, and found a number of regulatory proteins and putative cargoes associated with various AP complexes.

P34 regulates the stability of AP-1, AP-2 and AP-4

As the AP network had identified P34 as a hub protein interacting with several AP complexes, we investigated its function in *Arabidopsis*. Homozygous knockout *p34* mutants generated with the clustered regularly interspaced short palindromic repeats (CRISPR)/Cas9 technology (Extended Data Fig. 7a,b) could not be detected in the T1 generation nor in the offspring of two independent heterozygous lines, *p34-1(+/−)* and *p34-2(+/−)*. When grown in soil for 4 weeks, the rosette area of the heterozygous *p34-1(+/−)* and *p34-2(+/−)* mutants did not differ from the wild type (Extended Data Fig. 8a,b), but the siliques of the mature plants contained on average 25% abnormal seeds per silique, whereas only 0.5% of the seeds in the wild-type siliques were abnormal (Extended Data Fig. 8c,d). The absence of homozygous *p34* mutant plants and the observed 25% seed abortion suggest that the *P34* gene is essential for embryogenesis. Furthermore, we examined the embryogenesis in the *p34-2(+/−)* and found that embryo development is delayed in the *p34-2(−/−)* mutant seed (Extended Data Fig. 9e). At 14 days after pollination (DAP), approximately one-quarter of the seeds in the *p34-2(+/−)* mutant silique displayed shrinkage, indicating that P34 probably plays an important role in embryogenesis and embryo maturation (Extended Data Fig. 8e). Screening the CRISPR/Cas9 population revealed one biallelic *p34* mutant, designated *p34-3(Δ/−)*. The *p34-3(Δ/−)* mutant contained one allele with a nucleotide inserted 63 bp after the start codon, leading to a stop after the 30th amino acid and a second allele containing a 538 bp deletion and a 23 bp insertion, resulting in an in-frame

Fig. 4 | Validation of AP-5, AAK1, BAG4 and P34 protein interaction networks. **a**, Co-IP assays in tobacco leaves co-expressing different construct combinations. Free GFP was used as a negative control. White and black arrowheads indicate AP5B-RFP and AP5M-RFP, respectively. **b**, Quantification of rBiFC (YFP/RFP) between AP5M, AP5B and AP5Z. The interaction between AP5B and AP3B was used as a negative control. **c**, Cytoscape model of the AP-5 interactome. Edge colours represent the analysis methods used. **d**,**g**,**j**, Co-IP assays in *Arabidopsis* plants expressing *p35S:AAK1-GFP* (**d**), *p35S:BAG4-GFP* (**g**), *p35S:P34-GFP* (**j**) and *p35S:GFP* (**d**,**g**,**j**). AP-1, AP-2, TPC and clathrin were detected with α-AP1G, α-AP2A, α-AP2S, α-TPLATE and α-CHC antibodies. Free GFP was used as a negative control. Experiments were repeated three times independently, and one representative experiment is presented. **e**,**h**,**k**, Quantification of rBiFC (YFP/RFP) between AAK1 (**e**), BAG4 (**h**), P34 (**k**) and different AP subunits. The interactions between AP1G1 and AP3B and between AP1/2B1 and AP2A1 were used as negative and positive controls, respectively. Experiments were repeated twice, and one representative experiment is shown. *n* indicates number of cells. Significant differences were determined by one-way Brown–Forsythe and Welch ANOVA tests with Dunnett T3 multiple-comparisons test (**b**,**e**,**h** and **k**). $^{**}P \leq 0.01$ (**e**); $^{***}P \leq 0.001$ (**b**,**e**,**h** and **k**). NS, not significant (**b**, **e** and **h**). The bounds of boxes represents the 25th to 75th percentiles, the centre line indicates the median, and the whiskers indicate the minimum and the maximum values. All individual values were plotted. **f**,**i**,**l**, Cytoscape models of AAK1 (**f**), BAG4 (**i**) and P34 (**l**) protein interaction networks. Edge colours represent the analysis methods used. Node colours represent the different complexes and protein families: AP-1, red; AP-2, blue; AP-4, green; clathrin proteins, magenta; A/ENTH proteins, light green.

https://doi.org/10.1038/s41477-022-01328-2

translation of P34 with a deletion of 100 amino acids, from the 19th to the 118th amino acid (indicated as Δ) (Extended Data Fig. 7a,b). In contrast to the wild type and the two heterozygous *p34-1(+/−)* and *p34-2(+/−)* mutants, the *p34-3(Δ/Δ)* and *p34-3(Δ/−)* plants had smaller rosette areas when grown in soil (Extended Data Fig. 8a,b). The *p34-3(Δ/−)* mutant exhibited seed abortion rates similar to those of the heterozygous *p34-1(+/−)* and *p34-2(+/−)* alleles, whereas the *p34-3(Δ/Δ)* mutant behaved as the wild type (Extended Data Fig. 8c,d), suggesting that *p34-3(−)* and *p34-3(Δ)* are full knockout and hypomorphic alleles, respectively. Examination of the primary root length of seedlings grown in vitro for 7 days revealed that it was significantly reduced for the *p34-3(Δ/−)* mutant only (Extended Data Fig. 8f,g). Further complementation analysis of the *p34-1(+/−)* and *p34-3(Δ/−)* mutants with the *pP34:gP34:GFP* construct was carried out, and transgenic plants were recovered that resembled the wild-type plants in terms of rosette size, seed set and primary root length with the genotypes *pP34:gP34-GFP/p34-1(−/−)* and *pP34:gP34-GFP/p34-3(Δ/−)* (Extended Data Fig. 8a–g). As no homozygous *p34* mutant had been obtained and the biallelic *p34-3(Δ/−)* mutant did not allow genetic crossing, we generated β-oestradiol-inducible *ipRPS5A»CAS9-tagRFP-P34* knockout transgenic *Arabidopsis* plants

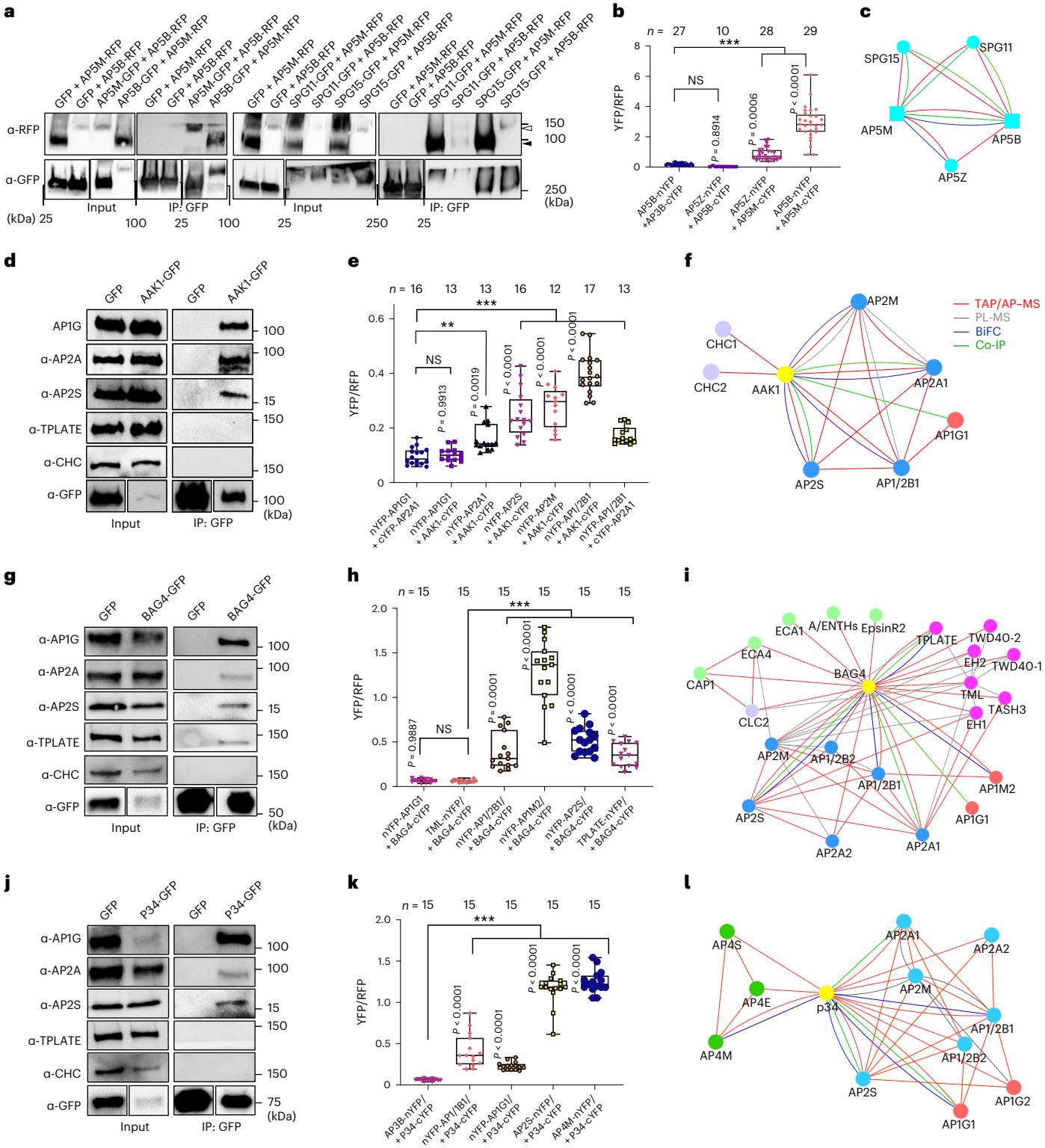

https://doi.org/10.1038/s41477-022-01328-2

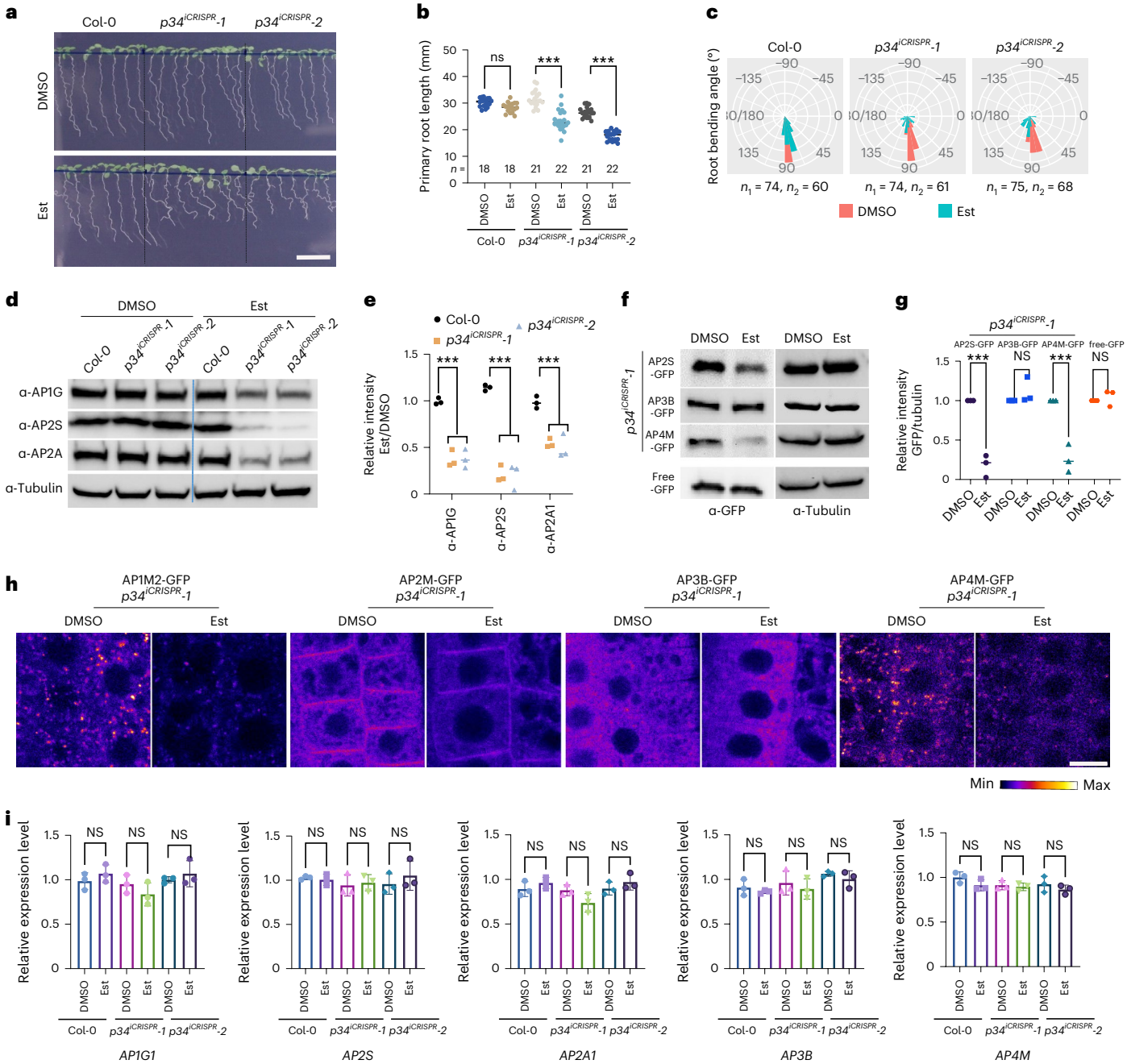

Fig. 5 | P34 regulates the stability of AP-1, AP-2 and AP-4. a, Wild-type (Col-0), *p34*^{iCRISPR}*-1* and *p34*^{iCRISPR}*-2* seedlings grown on medium containing DMSO (mock) or 10 μM β-oestradiol (Est) for 9 days. Scale bar, 10 mm. **b**, Primary root length of seedlings shown in **a**. *n* indicates number of roots. **c**, Root gravitropic bending of Col-0, *p34*^{iCRISPR}*-1* and *p34*^{iCRISPR}*-2* seedlings. Seven-day-old seedling grown as in **a** were gravistimulated by rotating 90° in two independent experiments. n_1 and n_2 indicate the number of roots treated with DMSO and Est, respectively. **d**,**e**, Protein levels of AP2S, AP2A1, AP1G and tubulin of seedlings in **a** analysed by immunoblotting. Relative quantities of target proteins were normalized to tubulin for each sample. The values were further normalized to the mock control for each genotype. Experiments were repeated three times. One representative experiment is shown. The quantification in **e** combines three independent experiments. **f**,**g**, Protein levels of AP2S-GFP, AP3B-GFP and AP4M-GFP in the *p34*^{iCRISPR}*-1* mutant analysed in 9-day-old *Arabidopsis* seedlings grown as in **a** by immunoblotting with α-GFP and α-tubulin. *35Sp:GFP* was used as a control. Relative protein levels of AP2S-GFP, AP3B-GFP and AP4M-GFP were normalized to tubulin. The quantification in **g** combines three independent experiments. **h**, Subcellular localization of AP1M2-GFP, AP2M-GFP, AP3B-GFP and AP4M-GFP in *p34*^{iCRISPR}*-1* mutant analysed in the root epidermis of 5-day-old *Arabidopsis* seedlings grown as in **a**. Scale bar, 10 μm. **i**, Expression levels of *AP1G1*, *AP2S*, *AP2A1*, *AP3B* and *AP4M* in 9-day-old seedlings grown as in **a**. RT–qPCR analysis was done in three independent experiments, each with three technical replicates. Transcript levels were normalized to *ACTIN2*. The significant differences were determined by one-way ANOVA test (**b** and **i**) and two-way ANOVA test (**e** and **g**). ***$P \leq 0.001$; NS, not significant. The *P* values versus the mock (**b**) for the Est-treated are Col-0 = 0.2207, *p34*^{iCRISPR}*-1* <0.0001 and the Est-treated *p34*^{iCRISPR}*-2* <0.0001. All *P* values versus Col-0 (**e**) are <0.0001. The *P* values versus the mock for different proteins in Est-treated *p34*^{iCRISPR}*-1* (**g**) are: AP2S-GFP <0.0001, AP3B-GFP 0.5996, AP4M-GFP <0.0001 and free GFP 0.9745.

(Fig. 5). Inference of CRISPR edits (ICE) analysis of two independent T2 lines, *ipRPS5A»CAS9-tagRFP-P34 #1-16* and *ipRPS5A»CAS9-tagRFP-P34 #5-12*, hereafter designated *p34*^{iCRISPR}*-1* and *p34*^{iCRISPR}*-2*, respectively, showed high genome editing on *P34* (Extended Data Fig. 9a). In addition, the P34-GFP signal in the *p35S:gP34-GFP/p34*^{iCRISPR}*-1* was almost eliminated after 5 days of β-oestradiol treatment (Extended Data

Fig. 9b). When grown on agar medium containing 10 µM β-oestradiol for 9 days, the primary root length of *p34*^{iCRISPR}*-1* and *p34*^{iCRISPR}*-2* plants were shorter than those of the dimethyl sulfoxide (DMSO) controls and of the β-oestradiol-treated wild type (Fig. 5a,b). Strikingly, the *p34*^{iCRISPR} mutants also exhibited an agravitropic root growth after induction (Fig. 5c).

Recently, the human P34/AAGAB has been reported to control the assembly and stability of AP-2 (ref. 42). To establish whether this is the case in plants, we assessed the protein levels of AP-1 and AP-2 in the inducible *p34*^{iCRISPR}*-1* and *p34*^{iCRISPR}*-2* mutants by immunoblots with α-AP1G, α-AP2A and α-AP2S antibodies (Fig. 5d,e). As anticipated, the AP1G, AP2A and AP2S protein levels were dramatically reduced in *p34*^{iCRISPR} mutants. Similar results were obtained in the biallelic *p34-3(Δ/−)* mutant but the protein levels of CHC and TPLATE in *p34-3(Δ/−)* were similar to those of the wild type (Extended Data Fig. 9c,d). We further tested whether the protein levels of AP-3 and AP-4 were also affected in the *p34* mutants. To this end, we crossed the *p34*^{iCRISPR}*-1* mutant with *pAP1M2:AP1M2-GFP/ap1m2-1*, *pAP2S:AP2S-GFP/ap2s*, *pAP2M:AP2M-GFP/ap2m-2*, *pAP3B:AP3B-GFP/pat2-1* and *pAP4M:AP4M-GFP/ap4m-2* and used the *p35S-GFP*/Col-0 plants as control. F2 seeds carrying the CRISRP/Cas9 construct were selected by seed fluorescence[51] and used for further experiments. Immunoblot analysis indicated that the levels of AP2S-GFP and AP4M-GFP, but not of AP3B-GFP and GFP, were reduced after β-oestradiol induction (Fig. 5f,g). In agreement, the protein abundance but not the subcellular localization of AP-1, AP-2 and AP-4 was altered in the *p34*^{iCRISPR}*-1* mutant (Fig. 5h). No significant difference in *AP1G1*, *AP2S*, *AP2A1*, *AP3B* and *AP4M* transcript levels were detected by quantitative reverse transcription polymerase chain reaction (RT–qPCR) analysis in the *p34*^{iCRISPR}*-1* mutant (Fig. 5i). Overall, our data show that P34 is an essential protein that controls the stability and possibly the assembly of AP-1, AP-2 and AP-4 but not of AP-3.

P34 modulates various vesicle trafficking pathways

We next examined whether P34 modulates the trafficking pathways mediated by AP-1, AP-2 and AP-4 as their abundance was affected when the P34 function was impaired. Consistent with previous studies in mammalian cells[42,43], P34-GFP mainly localized to the cytoplasm in the root cells and was not visibly associated with membranes or organelles (Extended Data Fig. 9e). First, we followed the general endocytosis by the FM4-64 uptake in *p34*^{iCRISPR}*-1* and *p34*^{iCRISPR}*-2* seedlings after β-oestradiol induction and in the *p34-3* mutants. The *ap2m-2* mutant was used as a reference. As expected, the internalization of FM4-64 in the root cells was significantly reduced in the *p34*^{iCRISPR} mutants (Fig. 6a,b). In addition, *p34-3(Δ/−)* also showed a decreased internalization of FM4-64 when compared with the wild type (Extended Data Fig. 9f,g).

Subsequently, the localization of the known CME cargo PIN2 (refs. 11, 37) in root cells of the *p34*^{iCRISPR} mutants was studied by whole-mount immunofluorescence labelling (Fig. 6c,d). The polar localization of PIN2 was severely disrupted, whereas its endosomal localization was more pronounced in the epidermal and lateral root cap cells. We also examined the accumulation of PIN2-GFP in Brefeldin A (BFA)-induced endosomal aggregates (so-called BFA bodies). No significant differences in PIN2-GFP BFA body size was observed between the wild type and the *p34*^{iCRISPR} mutants after a 1 h BFA treatment (50 µM) (Fig. 6e,f). In contrast, the dissipation of BFA bodies was significantly slower in the *p34*^{iCRISPR} mutant than in the wild type, as indicated by the retention of abundant BFA bodies in the *p34*^{iCRISPR} mutant after a 100 min BFA washout (Fig. 6e,g). These data indicate that P34 is essential for endocytosis, recycling, BFA-sensitive endosomal aggregation and polarity establishment of PIN2, probably through regulation of the AP-2 and AP-1 stability in the cytoplasm.

As AP-1 affects exocytosis, endocytosis and vacuolar trafficking[52], we investigated whether impairing the P34 function influences the trafficking of the secretory marker, secRFP[53], the PIN2 (ref. 37) and KNOLLE[7,49] proteins, and the localization of the TGN/EE-resident proteins, SYNTAXIN 61 (SYP61)[52] and VACUOLAR ATPASE SUBUNIT a1 (VHAa1)[52]. To this end, we assessed the secretion of secRFP to the apoplast in *p34*^{iCRISPR}*-1*. The localization of secRFP in the *p34* mutants after β-oestradiol induction remained apoplastic (Extended Data Fig. 10a), indicating that the secRFP secretion to the apoplast was not affected. By means of whole-mount immunofluorescence labelling, we determined the localization of KNOLLE during cytokinesis. In the wild type, KNOLLE is recruited to the developing cell plate via the secretory pathway[7], is targeted for vacuolar degradation once cytokinesis is completed[54] and is retrieved from the cell plate insertion site by endocytosis[25,55]. Although in the *p34*^{iCRISPR}*-1* plants some KNOLLE proteins reached the cell plate during and after cytokinesis, many more were detected in endosomes, possibly reflecting partial defects in its secretion and/or vacuolar trafficking (Extended Data Fig. 10b). Visualization of PIN2-GFP signals after dark treatment revealed that the PIN2-GFP accumulation in the vacuole was strongly reduced in the β-oestradiol-treated *p34* mutant similarly to the *ap1m2-1* mutant[7] (Extended Data Fig. 10c,d), further indicating that, besides secretion, vacuolar trafficking was also affected in the *p34*. Furthermore, when grown on DMSO, SYP61-CFP mainly localized to the TGN/EE in both wild-type and *p34*^{iCRISPR}*-1* root cells (Fig. 6h,i). However, after β-oestradiol induction, SYP61-CFP was mislocalized to the PM in the *p34*^{iCRISPR}*-1* line (Fig. 6h,i), likewise as when SYP61 was examined in the *ap1m2* mutant[52]. Moreover, the localization of VHAa1-RFP in *p34*^{iCRISPR}*-1* after β-oestradiol induction was not significantly altered (Fig. 6j,k) thus resembling the VHAa1 localization in the *ap1m2* mutant[52]. Taken together, these results suggest that in the *p34*^{iCRISPR} mutants some but not all aspects of AP-1-mediated trafficking are affected.

As impairment of the P34 function had an impact on the AP-4 stability, we studied the localization of the Epsin-like protein MODIFIED TRANSPORT TO THE VACUOLE1 (MTV1), previously shown to localize to the TGN/EE in an AP-4-dependent manner[23], in the *p34*^{iCRISPR}*-1* line (Fig. 6l,m). Similarly to its expression in the *ap4b-1* mutant, the punctate pattern localization of MTV1-GFP in the *p34*^{iCRISPR}*-1* mutant was reduced after β-oestradiol induction (Fig. 6l,m). Notably, in contrast to that in the *ap3* mutant[18], the vacuolar morphology remained unaffected and PIN2-GFP did not accumulate abnormally in the vacuole in *p34*^{iCRISPR}*-1* under normal light conditions (Fig. 6c and Extended Data Fig. 10e), suggesting that the AP-3-dependent pathway is functional.

All in all, our data demonstrate that P34 regulates CME to some extent but had a more pronounced impact on the trafficking to the vacuole and the localization of a subset of TGN/EE proteins, such as SYP61 and the AP-4 cargo MTV1, but not on the default secretion to the apoplast. We hypothesize that these results are achieved through maintenance of the correct protein levels of AP-1, AP-2 and AP-4 and possibly of their complex assembly.

Discussion

AP complexes are key regulators of the intracellular protein transport. AP dysfunction in mammalian cells disturbs many cellular processes, including organelle dynamics, tissue homeostasis and signal transductions, and provokes various heritable diseases and neurological disorders[3]. In plants, AP complexes also play critical roles in protein sorting and regulate several physiological processes[56]. Despite many similarities between plants and mammals, some structural differences make plant vesicle trafficking fundamentally distinct[4]. Firstly, the secretory as well as the endocytic pathway converge at the plant TGN/EE. Secondly, although plant cells rarely contain lysosomes, they possess large vacuoles with multiple functions. Thirdly, supposedly aiding to overcome the high turgor pressures, an actin-independent endocytic pathway combined with an additional membrane bending machinery, such as TPC, is evolutionarily retained in plants[4,26]. These differences imply plant-specific adaptations to control the vesicle trafficking mechanisms. (T)AP–MS and PL–MS methods have been routinely used for large-scale detection of protein–protein interactions in plants[28,36,57].

Both methods allow identification of protein interactions under near physiological conditions within a cell. Whereas (T)AP–MS reveals the binding partners in a stable protein complex, PL–MS identifies proteins that are in close proximity to the bait. The key advantage of (T)AP–MS is that it can be used to identify the core subunits and the accessory proteins of a complex. However, weak and transient interactors are often missing in the analysis. PL–MS is therefore developed as an alternative approach allowing the capture of such interactions. Previous studies[12,25] have already identified strong binders of AP-2 and TPL, demonstrating that possible CME cargoes could be discovered by means of PL-MS with AP2M and TML. In addition, a proteomic approach using purified CCVs coupled with a tandem MS analysis was also a powerful tool to identify the core and accessory machinery involved in CCV formation[35].

Mammalian AP-1, AP-2 and AP-3 interact with clathrin, whereas AP-4 and AP-5 do not[3], but only AP-1 and AP-2 are enriched in the mammalian CCVs and participate in their formation[3]. Although AP-3 can interact with clathrin, this interaction is currently viewed as non-essential under physiological conditions[58]. AP-5 does not require clathrin and instead associates with SPG11 and SPG15, which have been predicted to have α-solenoid structures similar to those of CHC, TPC and coatomer protein complex (COPI) subunits[59]. On the contrary, all subunits of AP-1, AP-2 and AP-4, but not those of AP-3 or AP-5, are enriched in plant CCVs[35]. The PL with TML identified CLC2 that, in agreement with previous reports, connects TPC with clathrin[25]. In our interactome, however, no clathrin associated with any of the five AP complexes. Conversely, TAP–MS detected CHC1 and CHC2 associated with the AP-2 binding partner, AAK1, whereas CLC1 and CLC2 associated with the AP-1 and AP-2 binding partner, BAG4. Nevertheless, these interactions were not confirmed by the co-IP experiments.

Human AAK1 regulates CME by phosphorylating the medium subunit of AP-2, which promotes binding of AP-2 to cargo proteins during CCV formation[44,60]. This kinase modulates several pathways, including NOTCH and WNT signalling[44,45,61]. The AP-2 network showed that *Arabidopsis* AAK1 binds specifically to AP-2, suggesting that AAK1 might regulate AP-2 functions and CME in plant cells. AAK1 also interacted with BAG4, which had been identified as a hub protein associated with AP-1, AP-2 and TPC. The BAG family is evolutionarily conserved in eukaryotes, and the human BAG proteins act as co-chaperones of the heat shock protein (HSP)70 family. BAG4 proteins are involved in multiple functions, such as apoptosis, autophagy, proteasomal and lysosomal degradation, neurogenesis and tumourigenesis[62]. *Arabidopsis* contains seven BAG family members, and BAG4 was shown to be involved in salt responses and stomatal movement[41]. Consistent with the obtained protein–protein interaction data, BAG4 also associated with clathrin, TOM1-LIKE (TOL) ESCRT-0 proteins[63,64], two ANTH-type clathrin adaptors, ECA4 and CAP1 (ref. 25) and a group of HSPs[41], hinting at a role for the *Arabidopsis* BAG4 in protein degradation linked either to autophagy, the ubiquitin-mediated proteasomal degradation pathway or endocytosis[64,65].Taken together, our data uncover an intimate network of the AP-1, AP-2, TPC, AAK1, BAG4 and the A/ENTH proteins that are involved in clathrin-dependent protein trafficking. The AP interactome revealed that in *Arabidopsis* AP-3, AP-4 and AP-5 are more closely related to each other, not only because they share several interacting components but also because some of their subunits co-purified. Instead of acting in a clathrin-dependent manner, human AP-5 cooperates with SPG11 and SPG15 as a scaffold and a docking site, respectively[46]. We discovered that the *Arabidopsis* AP-5 also associates with the plant homologues of human SPG11 and SPG15, AT2G25730 and AT4G39420, respectively, of which the functions in plants are still not elucidated. In spite of the high probability that *Arabidopsis* AP-5 also acts together with SPG11 and SPG15 in plants, we could not exclude that AP-5 might utilize or share subunits with AP-3 and/or AP-4, because the AP5S subunit gene is absent in the *Arabidopsis* genome and the three AP complexes crosstalk during the trafficking between TGN and late endosomes in plant cells. In addition, our interactome identified significant but weak interactions between subunits of different AP complexes (Extended Data Fig. 1). Such interconnections are typically represented by substoichiometric interactions, whereas interactions within the core AP complexes were much more abundant and stoichiometric. Whether the interactions between subunits of different AP complexes are physiologically relevant remains unclear. AP subunits share similar structural folds, which might provide an affinity for one another. Therefore, it is possible that overexpression of one subunit as a bait can generate an imbalance with respect to other endogenous subunits, allowing artificial interactions between complementary AP subunits.

Furthermore, we discovered one important regulatory protein that links the functions of AP-1, AP-2 and AP-4 in plant, *Arabidopsis* P34. In humans, P34/AAGAB controls the sequential assembly of AP-1 and AP-2, but not that of AP-3 (ref. 42), and it is still unclear whether P34 regulates AP-4 or AP-5. *Arabidopsis* P34 positively regulated the stability of AP-1 and AP-2, whereas the AP-3 stability remained unchanged in the *p34* knockout mutants, consistently with the results in human cells. In *Arabidopsis*, P34 also interacted with the AP-4 subunits (AP4E, AP4M and AP4S) and the AP4M protein was notably reduced in the *p34* mutant. In contrast, P34 did not co-purify with TPC, implying that in plants it directly regulates the protein stability of the three clathrin-associated AP complexes, AP-1, AP-2 and AP-4 (ref. 35) but not that of AP-3 and TPC. Therefore, P34 might be a regulator of multiple clathrin-mediated vesicle trafficking pathways in *Arabidopsis*. Although debatable, some evidence exists that the activities of clathrin-dependent post-Golgi trafficking and CME are highly coordinated in plant cells[52,66]. Recently, the recruitment of several endocytic components to the PM, including CLC1, CHC1, AP2M, AP2S, TPLATE and TML, was shown to be reduced in the *ap1m2* mutant, but their protein levels to remain unchanged[52]. Similarly, in mutants defective in AP-2 and TPC-dependent CME, the clathrin and AP-1 recruitment to the TGN/EE as well as exocytosis are impaired[52]. As the impaired P34 function strongly affected the protein levels of the AP-1, AP-2 and AP-4 subunits and probably other CME components, we hypothesized that multiple trafficking pathways would be affected in the *p34* mutant.

Fig. 6 | P34 regulates vesicle trafficking depending on AP-1, AP-2 and AP-4. **a**, Root epidermis of 5-day-old Col-0, *p34*^{iCRISPR}*-1*, *p34*^{iCRISPR}*-2* and *ap2m-2* seedlings grown on medium containing DMSO (mock) or 10 μM β-oestradiol (Est) were imaged after staining with FM4-64 (2 μM, 15 min). **b**, Relative PM to intracellular fluorescence intensity ratio of FM4-64 of images in **a**. Ten roots were analysed. **c**,**d**, Immunolocalization of PIN2 in epidermal (epi) and cortex (cox) cells (**c**) and in lateral root cap (LRC) cells (**d**) of 7-day-old Col-0, *p34*^{iCRISPR}*-1* and *p34*^{iCRISPR}*-2* roots treated with Est. Arrowheads and arrows indicate the PM-localized PIN2 and endosomal PIN2, respectively. The insets show the polarity of PIN2 in the epidermis. The ratio of PIN2 abnormal/normal localization in roots is indicated for three independent experiments. **e**, BFA washout experiment of PIN2-GFP in 5-day-old wild-type and *p34*^{iCRISPR}*-1* roots grown as in **a**. **f**, BFA body sizes before the washout. *n* indicates number of BFA bodies. At least seven roots were measured. **g**, Percentage of BFA-body-containing cells in PIN2-GFP seedlings before and after BFA washout in **e**. **h**, Fluorescence intensity images of SYP61-CFP in the root cells of 5-day-old Col-0 and *p34*^{iCRISPR}*-1* grown as in **a**. **i**, PM/intracellular fluorescence intensity ratios of SYP61-CFP in one representative experiment. At least five roots were measured. **j**, Fluorescence intensity images of VHAa1-mRFP in the root cells of 5-day-old Col-0 and *p34*^{iCRISPR}*-1* grown as in **a**. **k**, PM/intracellular fluorescence intensity ratios of VHAa1-mRFP in one experiment. **l**, Localization of MTV1-GFP in the root cells of 5-day-old Col-0, *p34*^{iCRISPR}*-1* and *ap4b-1* grown as in **a**. **m**, Quantification of the presence of defined MTV1-GFP punctate signals by analysis of the skewness of the signal intensity from at least seven roots. Higher skewness indicates more diffuse signals. Experiments were repeated three times. One representative experiment is shown. Data are presented as mean values (centre line). Error bars represent standard deviation. ***$P \leq 0.001$ (one-way ANOVA (**b**,**f**,**i**,**k** and **m**)). *n* indicates number of roots (**g** and **m**) or cells (**i** and **k**) analysed. NS, not significant. AU, arbitrary units. Scale bars, 10 μm (**a**,**c**,**d**,**e**,**h**,**j** and **l**).

https://doi.org/10.1038/s41477-022-01328-2

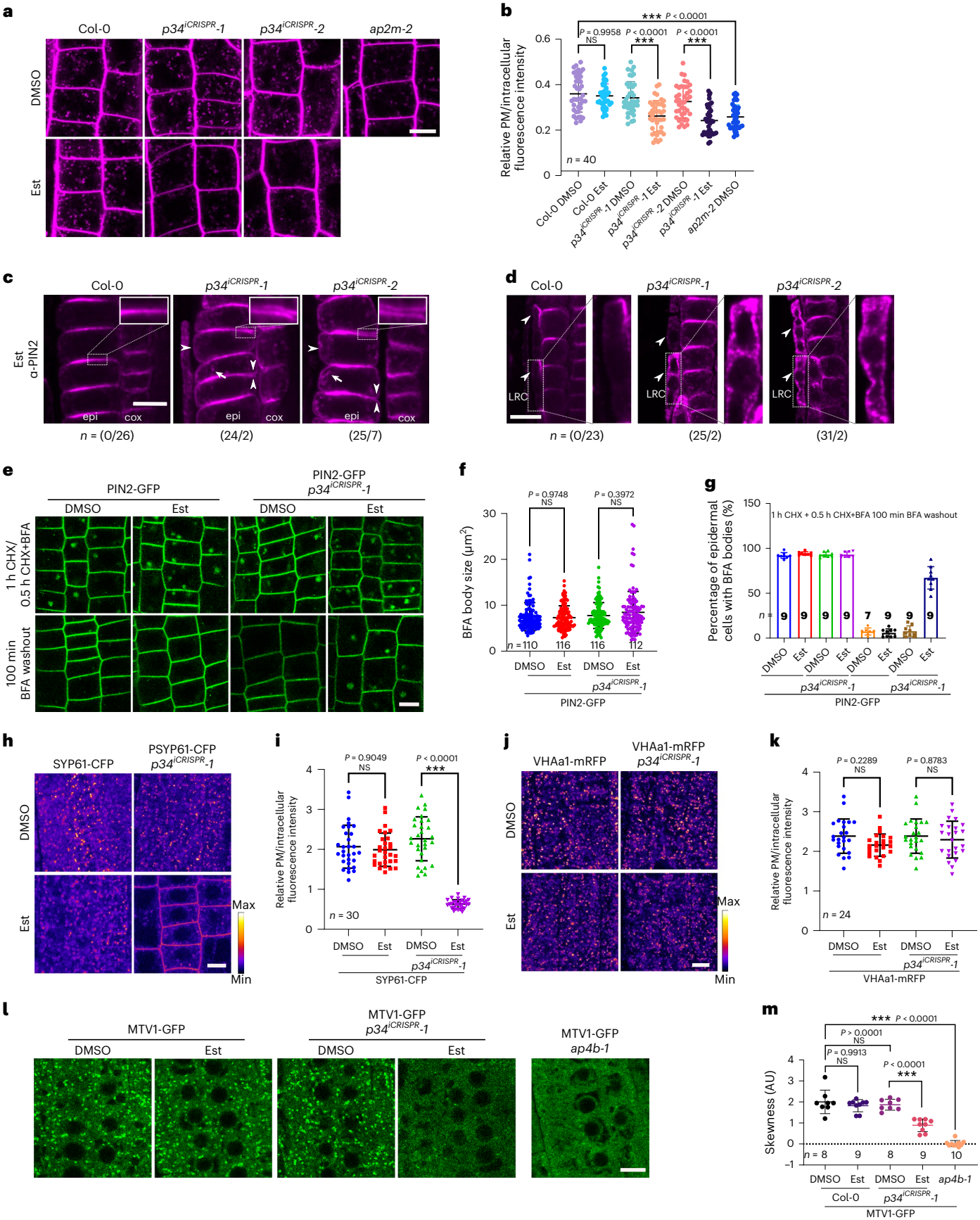

Indeed, as predicted, the internalization of the lipophilic PM tracer dye FM4-64 was reduced in the *p34* mutant and the localization of the TGN/EE-resident protein SYP61 was altered similarly to that in *ap1m2* (ref. 52), suggesting that P34 regulates the trafficking pathways controlled by AP-1 and AP-2. Why SYP61 is mistargeted to the PM when the AP-1 function is impaired remains to be determined, but in the absence of degradation, SYP61 might be assumed to be targeted by default to the PM. PIN2 polarization and recycling from BFA-sensitive endosomes were also defective in *p34*. Previously, modification of the PIN2 polar localization in the cells of staminal filaments of *ap2m-1* (ref. 11), and decrease in the recycling of PIN2 from the BFA-sensitive endosome in mutants of AP-1 and AP-2 subunits have been shown[9,52]. In addition, a more diffuse endosomal KNOLLE signal was observed in *p34*, reminiscent of the KNOLLE localization in *ap1m2-1* (ref. 8). The lack of ectopic KNOLLE localization at the post-cytokinetic cell wall insertion site indicates that *p34* is a weaker mutant than *ap1m2*, without impact on sterol- and TPC-dependent endocytosis[53,67]. Consistently, the secretory marker secRFP was correctly transported to the apoplast in *p34*, but was impaired in the *ap1m2* mutants[7,52]. Previously, AP-1 and AP-4 have been reported to localize in different subdomains of TGN/EE[23], and to initiate secretory and vacuolar trafficking from different subregions of TGN/EE[5]. P34 directly regulated the function of AP-4, because the TGN/EE-resident protein MTV1 that requires the AP-4 function for its localization[23] was mislocalized and mostly remained cytosolic in *p34*. The differences between the *p34* and *ap1* mutants might therefore be linked to the TGN integrity that might be more affected in *ap1* than in *p34*.

In summary, the generated AP interactome provides useful resources to discover unknown regulators or co-operators of the AP complexes that might be unique to plant cells or have a common function in all eukaryotic cells, such as AAK1, P34, SPG11 and SPG15. Our findings identified P34 as a regulator of clathrin-mediated post-Golgi transport and CME by abundance maintenance of the AP-1, AP-2 and AP-4 complexes in plant cells. Which factors regulate the stability and possibly the assembly of TPC, AP-3 and AP-5 in *Arabidopsis* remains to be determined.

Methods

Plant material and growth conditions

Arabidopsis thaliana (L.) Heynh., accession Columbia-0 (Col-0), plants were used for all experiments. *Arabidopsis* seeds were sown on half-strength Murashige and Skoog (½MS) agar plates without sucrose or in liquid ½MS without sucrose and vernalized at 4 °C under dark conditions for 3 days. Seeds were germinated and grown at 22 °C and a 16 h light/8 h dark photoperiod for 5, 7 or 9 days, according to the experimental purposes. For *P34*-inducible CRISPR editing experiments, seeds were germinated and grown directly on ½MS containing either DMSO or 10 µM β-oestradiol at 22 °C and a 16 h light/8 h dark photoperiod for 5, 7 or 9 days. Transgenic *Arabidopsis* lines expressing *p35S:GFP/Col-0* (ref. 68), *pAP1M2:AP1M2-GFP/ap1m2-1* (ref. 69), *pAP2S:AP2S-GFP/ap2s*[15], *pAP2M:AP2M-GFP/ap2m-2* (ref. 16), *pMTV1:MTV1-GFP/Col-0* (ref. 23), *pMTV1:MTV1-GFP/ap4b-1* (ref. 23), *pAP4M:AP4M-GFP/ap4m-2* (ref. 70), *pAP3B:AP3B-GFP/pat2-1* (ref. 18), *pSYP61:SYP61-CFP*[71], *pVHAa1-VHAa1-mRFP*[72], *p35S:secRFP*[51], *pPIN2:PIN2-GFP*[37], *ap2m-2* (ref. 16) and *ap4m-2* (ref. 70) have been previously described. Wild-type tobacco (*Nicotiana benthamiana*) plants were grown in the greenhouse under a normal 14 h light/10 h dark regime at 25 °C.

Rosette area measurements

Four-week-old plants grown in soil in multipot trays were imaged. The total leaf area of individual plants was selected by means of the ImageJ colour threshold tool. Per genotype, eight to nine seedlings were planted randomly to exclude position effects. The experiments were repeated three times independently. The rosette area from a total of 24–25 plants per genotype was measured.

Generation of constructs and transformation

For the entry clones, genomic DNA of *Arabidopsis AP1G1*, *AP1G2*, *AP1S1*, *AP2S*, *AP3B*, *AP4E*, *AP4S*, *AP5B*, *AP5M*, *P34*, *BAG4*, *AAK1*, *SH3P1*, *NECAP-1*, *ECA1*, *ECA4* and *CAP1* were cloned into a Gateway entry vector *pDONR221* with a BP reaction. For the TAP–MS and AP–MS constructs, the above genes were fused N-terminally or C-terminally to the GS^{TEV} or GS^{rhino} TAP tag under control of the *35S* promoter by subcloning the entry clones into *pKCTAP* or *pKNGSrhino/pKNGSTAP*[73] using Gateway. For *p35S:AAK1-GFP*, *p35S:BAG4-GFP*, *p35S:P34-GFP* transgenic *Arabidopsis*, the genomic DNA of *AAK1* and *P34* and the complementary DNA of *BAG4* were first cloned into *pDONR221*, then subcloned into the binary Gateway vector *pK7FWG2* (ref. 73) and finally transformed into *Arabidopsis* Col-0 by floral dip. For the co-IP experiments, entry clones of *AP3B*, *AP4E*, *AP5B* and *AP5M* were subcloned into *pK7FWG2* (ref. 73) to generate the *p35S:AP3B-GFP*, *p35S:AP4E-GFP*, *p35S:AP5B-GFP* and *p35S:AP5M-GFP* constructs or subcloned into *pH7RWG2* (ref. 73) to generate the *p35S:AP5B-RFP* and *p35S:AP5M-RFP* constructs. Genomic DNA of *SPG11* and *SPG15* were cloned into *p35S:GFP-pGGK* vector by Gibson assembly using SalI cutting site to generate the *p35S:SPG11-GFP* and *p35S:SPG15-GFP* constructs. *p35S:GFP-pGGK* was created by the Golden Gate system with *pGG-A-35SP-B*, *pGG-B-Linker-C*, *pGG-C-GFP-D*, *pGG-D-35ST-G* and *pGGK-AG*. For the *p35S:P34-mCherry* construct, cDNA of *P34* was cloned into *pGGB000* and subcloned into the backbone vector *pFASTRK-AG* and *pGG-AG-KmR* by the Golden Gate system with *pGG-A-35SP-B, pGG-C-mCherry-D or pGG-C-GFP-D* and *pGG-D-35ST-G*[74]. To generate the *pP34:gP34-GFP* construct, the promoter (1,812 bp) and genomic DNA (2,035 bp) of *P34* were cloned into the *pDONR P4-P1r* and *pDONR221* vectors, respectively, and then subcloned into the *pH7m34GW* vector with *pDONR P2R-P3-EGFP* by means of the MultiSite Gateway system. The rescued lines were generated by transforming the *pP34:gP34-GFP* construct into *p34-1(+/−)* and *p34-3(Δ/−)* plants by floral dip.

For the CRISPR/Cas9 constructs, two guide RNAs (gRNAs) that targeted the first and the last exon of *P34* were designed with the 'CCtop' software (https://cctop.cos.uni-heidelberg.de:8043/)[75]. The two gRNAs (Supplementary Table 4) were cloned into the entry vectors *pGG-C-AtU6-26-BbsI-ccdB-BbsI-D* and *pGG-D-AtU6-26-BbsI-ccdB-BbsI-E*[74]. The CRISPR/Cas9 expression construct was generated by assembling the entry clones with *pGG-A-linkerIII-C*, *pGG-E-linker-G*[76], into the backbone vector *pFASTRK-Atcas9-AG*[49] with the Golden Gate reaction. For the inducible CRISPR construct, the entry clones of the gRNAs and *pGG-A-linkerIII-C*, *pGG-E-linker-G* were first cloned into the *pEN-R2-AG-L3* (ref. 77) with the Golden Gate reaction. The resulting *pEN-R2L3-gRNA* constructs were then subcloned with *pEN-R4-RPS5A-XVE-L1* (ref. 65) and *p221z-CAS9p-tagRFP* into the *pK8m43GW* binary vector by a Multisite Gateway reaction. The CRISPR and inducible CRISPR expression constructs were then transformed into Col-0 by floral dip. For genotyping, the genomic DNA sequence of *P34* of the transgenic plants was amplified by PCR with the primers listed in Supplementary Table 4.

For the rBiFC assay[78], cDNA of *BAG4*, *P34*, *AAK1*, *AP1M2*, *AP4M*, *AP5M*, *AP5Z*, *AP5B*, *FH6*, *KNOLLE* and *BIN2* were first cloned into *pDONR-p3p2* or *pDONR-p1p4* to generate the entry clones. The entry clones were then subcloned with *pDONR-p3p2-AP2S*, *pDONR-p3p2-AP1G1* or *pDONR-p3p2-AP2A1*, *pDONR-p3p2-AP12B1* and *pDONR-p3p2-AP2M*[13] into the expression vectors *pBiFC-2in1-NN*, *pBiFC-2in1-CN*, *pBiFC-2in1-NC* or *pBiFC-2in1-CC*[78] by Multisite Gateway cloning. All primers used for cloning are listed in Supplementary Table 4.

Chemical treatments

β-oestradiol (Sigma-Aldrich, 20 mM stock in DMSO), BFA (Sigma-Aldrich, 50 mM stock in DMSO), cycloheximide (CHX) (Merck, 50 mM stock in DMSO) and FM4-64 (Invitrogen, 2 mM stock in water) were used at the concentrations indicated. For the BFA washout, seedlings were first treated with CHX (50 µM) for 1 h and then with CHX (50 µM) and BFA (50 µM) for 30 min. Seedlings were washed with medium containing CHX (50 µM) and imaged 100 min after the wash.

rBiFC analysis and quantification

For the rBiFC assay, the *Agrobacterium tumefaciens* strain C58 carrying the 2in1 constructs[78] were co-infiltrated with a p19-carrying strain into tobacco leaves and incubated in the greenhouse for 2 days. Afterwards, infiltrated leaves were observed either with an SP8 (Leica) or Fluoview1000 (Olympus) confocal microscope. The rBiFC analysis was quantified by means of 8-bit greyscale images containing less than 1% saturated pixels. The PM was outlined with the selection brush tool in Fiji, and the mean intensity of the selected region of interest was calculated in both channels to generate an YFP/RFP ratio per cell. All rBiFC combinations tested are listed in Supplementary Table 2.

TAP, single-step affinity purification and PL experiments

All GS^{TEV} and GS^{rhino} TAP tag fusion constructs were transferred to the *Agrobacterium* C58C1 strain pMP90 for transformation into the PSB-D *Arabidopsis* cell culture. The transformed *Arabidopsis* cells were cultured and collected, followed by protein complex purification and liquid chromatography with tandem MS identification of the purified proteins[57]. For proximity biotinylation experiments[36], AP2M and TML were combined C-terminally with TurboID and a 65-amino-acid linker sequence in between[36]. *Arabidopsis* cells were transformed according to the procedure for the TAP purifications. Biotinylated proteins were purified and identified by growing the cell cultures at 28 °C, incubating them for 24 h with 50 µM exogenous biotin, extracting the proteins under very harsh conditions (100 mM Tris (pH 7.5), 2% (w/v) SDS and 8 M urea) and a two-step elution, followed by liquid chromatography with tandem MS analysis on a Q Exactive (Thermo Fisher Scientific). Protein sequences were aligned with CLC (Qiagen CLC Main Workbench 8.1) software, and gene accession numbers are listed in Supplementary Table 5.

TAP–MS, AP–MS and PL–MS analysis and background filtering

Two and three replicates were done for TAP and single-step AP, respectively. After each set of two TAP or three AP purifications, the identified protein list was filtered versus a list of non-specific proteins, assembled from a large dataset of TAP–MS or AP–MS experiments[72]. All proteins appearing with three or more bait groups in the large dataset were included in a list of non-specific proteins. For each TAP–MS set of two experiments to be analysed, the background was marked in the list of the co-purified proteins. To prevent that true interactors were filtered out because of their presence in the list of non-specific proteins, the ratio was calculated of the average normalized spectral abundance factors (NSAFs) of the identified proteins in the bait pull-downs versus the corresponding average NSAFs in a large control set of pull-downs. Proteins identified with at least two peptides in at least two experiments, which did not occur in the background list, or showed a high (at least 20-fold) enrichment versus the large dataset of TAP experiments, were retained. Identifications without high enrichment versus the large dataset were removed, unless they were present in one of the other TAP–MS experiment sets. For each AP–MS set of three experiments to be analysed, the same approach was followed, additionally with a Student's *t*-test. Identifications with a high (NSAF ratio ≥10) and significant (−log(*P* value) ≥10) enrichment versus the large control AP–MS dataset were retained. The PL–MS data were filtered by comparison with a PL–MS control dataset built from experiments done under the same conditions. Identifications with enrichment score (ES) ≥20 were considered enriched, namely ES = NSAF ratio × −log(*P* value). Protein interactions were visualized in networks with the Cytoscape v3.7.2 software using the input in Supplementary Table 1 or in a dot plot matrix with ProHits-viz[79].

Gene set enrichment analysis

Gene set enrichment was analysed with ShinyGO v0.741:Gene Ontology Enrichment Analysis + more (http://bioinformatics.sdstate.edu/go/)[80] in *Arabidopsis* with a *P*-value cut-off (false discovery rate (FDR)) of 0.05 and the top 30 pathways. The networks of enriched GO terms were visualized with the Cytoscape v3.7.2 software. Two terms were connected when they shared 20% or more genes. The fold change of each term was indicated by the size of the nodes, and the number of shared genes between two terms was indicated by the line thickness.

Immunohistochemistry

Immunolocalizations were carried out on 7-day-old or 9-day-old seedlings grown on ½MS medium containing 10 µM β-oestradiol by means of the immuno-robot InsituPro Vsi II (Intavis)[81]. In brief, the samples were fixed by paraformaldehyde (4% (v/v)) in phosphate-buffered saline (PBS) for 1 h in vacuum. After fixation, the samples were transferred to the robot and subsequently subjected to six washes (three times in PBS, pH 7.4, and 0.1% (v/v) Triton X-100 (PBS-T) and three times in distilled water with 0.1% (v/v) Triton X-100; 5 min each), cell wall digestion (1.5% (w/v) driselase in PBS, for 30 min at 37 °C), three washes (PBS-T, for 5 min), permeabilization (3% (v/v) NP-40, 10% (v/v) DMSO in PBS; for 30 min at room temperature), three washes (PBS-T, for 5 min), blocking solution (3% (w/v) bovine serum albumin in PBS, for 1 h at 37 °C), primary antibody solution (primary antibodies diluted in blocking solution, for 4 h at 37 °C), five washes (PBS-T, for 5 min), secondary antibody solution (secondary antibodies diluted in blocking solution, for 3 h at 37 °C), five washes (PBS-T, for 5 min); when 4′,6-diamidino-2-phenylindole (DAPI) staining was needed, samples were incubated in 1 µl DAPI in stock with 5 ml distilled water for 15 min, followed by five washes with distilled water for 5 min. The dilutions of the primary antibodies were: rabbit α-PIN2 (1:600)[49,82] mouse α-tubulin (Sigma-Aldrich, T5168) (1:1,000), rabbit α-Knolle (1:1,000) (kind gift from Dr Gerd Jürgens) and of the secondary antibodies: AlexaFluor488 goat α-mouse (1:600) (A-11001, Thermo Fisher Scientific) and AlexaFluor555 donkey α-rabbit (1:600) (A-31572, Thermo Fisher Scientific). The DAPI (D9542, Sigma-Aldrich) stock concentration was 1 mg ml^{-1}.

Gravitropic responses

Five-day-old Col-0, *p34*^{iCRISPR}*-1* and *p34*^{iCRISPR}*-2* seedlings, light-grown vertically on medium supplemented with DMSO or 10 µM β-oestradiol, were gravistimulated by a 90° rotation. The angle of the root tips deviating from the vertical plane was measured with the ImageJ (http://rsb.info.nih.gov/ij/) software 24 h after gravistimulation. Gravicurvature was quantified in two independent experiments with a total of 61–74 roots. All gravitropically stimulated roots were assigned to a gravitropism diagram by an online tool (https://rmtrane.shinyapps.io/RootNav/).

RT–qPCR

RNA was extracted from 9-day-old seedlings with the ReliaPrep RNA Miniprep Systems (Promega). Of purified RNA, 1 µg was amplified in a reverse transcriptase reaction with the qScript XLT 1-Step RT-PCR Kit (Quantabio). Subsequently, qPCR was run with the SYBR Green master mix (Roche) with gene-specific primers designed to amplify *AP1G1*, *AP2S*, *AP2A1*, *AP3B* and *AP4M*. *ACTIN2* was used as the normalization reference. Primers are listed in Supplementary Table 4.

Embryo analysis

Embryogenesis was observed as previously described[83]. In brief, flowers of Col-0 and *p34-2(+/−)* plants were self-pollinated. Fresh ovules were dissected from siliques at 6, 7 and 14 DAP and cleared in Hoyer's solution (24 g of chloral hydrate with 9 ml ultrapure water and 3 ml of glycerol). The cleared ovules were viewed under Olympus BX51 microscope with differential interference contrast optics.

Protoplast isolation and transfection

Arabidopsis protoplasts were isolated from 14-day-old seedlings as previously described[84]. Briefly, *ap4m-2* mutant seedlings were cut into strips in TVL buffer (50 mM $CaCl_2$ and 0.3 M sorbitol) and then

digested in enzyme buffer (0.5 M sucrose, 20 mM $CaCl_2$, 40 mM KCl, 1% (w/v) Cellulase R-10, 1% (w/v) Macerozyme R-10 and 10 mM MES at pH 5.7) with gentle shaking for 16 h in the dark. The protoplasts were collected by centrifugation at 100*g* for 7 min and washed twice with W5 buffer (0.1% (w/v) glucose, 0.08% (w/v) KCl, 0.9% (w/v) NaCl, 1.84% (w/v) $CaCl_2$, and 2 mM MES at pH 5.7). Then the protoplasts were transfected with *p35S:p34-GFP* or *p35S:GFP* using PEG solution (40% (w/v) PEG 4000, 0.2 M mannitol and 0.1 M $CaCl_2$) and then incubated at room temperature for 15 min in the dark. The transfection was stopped by adding W5 buffer. The protoplasts were pelleted by centrifugation at 100*g* for 3 min and resuspended gently in W5 buffer. The protoplasts were then transferred into multi-well plates and incubated in the dark overnight at room temperature.

Co-IP assay

For co-IP, 7-day-old *Arabidopsis* seedlings were collected and ground into powder with liquid nitrogen. The powder was resuspended in extraction buffer (50 mM Tris–HCl, pH 7.5, 150 mM NaCl, 0.5% (v/v) NP-40, and complete EDTA-free protease inhibitor cocktail (Roche)).

For co-IP in tobacco, *Agrobacterium* cultures carrying the indicated constructs were resuspended in infiltration buffer (10 mM $MgCl_2$, 10 mM methyl ethyl sulfide, pH 5.6, and 100 µM acetosyringone) and incubated at room temperature for 2 h. The bacterial cultures were adjusted to a final OD_{600} of 0.5 for each construct and infiltrated into tobacco leaves. Tobacco leaves were collected 3 days after inoculation and ground into powder with liquid nitrogen and then resuspended in extraction buffer [150 mM Tris–HCl, pH 7.5, 150 mM NaCl, 10% (v/v) glycerol, 10 mM EDTA, 1% (v/v) NP-40, and complete EDTA-free protease inhibitor cocktail (Roche)]. The extracts were centrifuged twice at 20,000*g* at 4 °C for 15 min. The supernatants were incubated with GFP-trap magnetic agarose (Chromotek) at 4 °C for 2 h. Beads were washed three times with 1 ml wash buffer (20 mM Tris–HCl, pH 7.5, 150 mM NaCl and 0.25% (v/v) NP-40) followed by SDS–PAGE analysis.

SDS–PAGE and immunoblotting

Total protein extracts were obtained by grinding the plant materials into a fine powder with liquid nitrogen. The powder was resuspended in extraction buffer (50 mM Tris–HCl, pH 7.5, 150 mM NaCl, 0.5% (v/v) NP-40, and complete EDTA-free protease inhibitor cocktail (Roche)). The extracts were centrifuged twice at 20,000*g* at 4 °C for 15 min. The protein extracts were boiled in sample buffer (1× NuPAGE LDS sample buffer, 1× NuPAGE Reducing Agent (Thermo Fisher Scientific)) for 10 min at 90 °C and loaded on 4–20% (w/v) Mini-PROTEAN TGX Precast Protein Gels (Bio-Rad). The proteins were separated by electrophoresis and blotted onto a membrane with trans-Blot Turbo Mini 0.2 µm Nitrocellulose Transfer Packs (Bio-Rad). Membranes were blocked overnight at 4 °C in 3% (w/v) skimmed milk dissolved in 25 mM Tris–HCl (pH 8), 150 mM NaCl and 0.05% (v/v) Tween20. The blots were then incubated at room temperature with the monoclonal α-GFP antibody (1:5,000) (Miltenyi Biotec, 130-091-833), α-RFP antibody (1:5,000) (ChromoTek, α-RFP antibody (6G6)), α-AP2S antibody[85] (1:500), α-AP2A antibody[86] (1:2,000), α-AP1G antibody[87] (1:2,000), α-tubulin antibody (Sigma-Aldrich, T5168) (1:2,000), α-CHC antibody (1:2,000) (Santa Cruz, sc-57684) and α-TPLATE antibody (1:500)[88]. The secondary antibodies are ECL α-Rabbit IgG (Amersham, NA934V) (1:10,000) and ECL α-Mouse IgG (Amersham, NXA931V) (1:10,000). The blots were imaged and analysed by Image Lab Software 3.0 (Bio-RAD).

ICE analysis

The Sanger trace data of 9-day-old $p34^{iCRISPR}$-*1* and $p34^{iCRISPR}$-*2* plants were analysed with the online ICE Analysis Tool v3.0 (https://ice.synthego.com/). The percentage of genomic DNA sequences that contain an insertion or deletion in the sample is represented by indel %, whereas the knockout score corresponds with the proportion of sequences that will probably result in a functional protein knockout.

Confocal microscopy and image quantification

All the confocal images, except Extended Data Fig. 7, were acquired with a Leica SP8X confocal microscope with application of the gating system (0.3–6 ns) for autofluorescence removal. GFP, YFP, RFP and FM4-64 were excited by white laser. The excitation and detection window settings were: GFP, 488/500–530 nm; YFP, 514/525–555 nm; RFP, 561/600–650 nm; and FM4-64, 515/570–670 nm. CFP was excited by diode at 405 nm and collected at 460–500 nm. Confocal images in Extended Data Fig. 6d were acquired with an inverted Olympus Fluoview1000 confocal microscope by means of line sequential imaging at a resolution of 512 × 512 pixels, 8 µs per pixel scan speed, 4× line averaging, one-way scan direction, and an UPSLAPO 60× water immersion corrected lens (numerical aperture 1.20). The YFP and RFP channels were imaged with a 515 nm laser line from an argon laser (85% intensity) and a 559 nm solid state laser (10% intensity) and emission windows between 530 nm and 548 nm and between 580 nm and 615 nm, respectively. Confocal images in Fig. 6c,d and Extended Data Fig. 10b were acquired with a Zeiss LSM710 confocal laser scanning microscope equipped with a 40× water-corrected objective for detection of Alexa488 (488/500–545 nm), Alexa555 (561/555–610 nm) and DAPI (358/461 nm). For BFA body size and BFA body number analyses (Fig. 6e) and for visualization of PIN2-GFP in vacuoles after dark treatment (Extended Data Fig. 10c), four images of root epidermal cells each with a 2.5 µm *Z*-axis distance were taken and stacked together before quantification[89]. The fluorescent PM intensity and intracellular space were measured with ImageJ for the quantification of the FM4-64 uptake and the SYP61-CFP and VHAa-RFP signals. The relative fluorescent cytoplasm/PM intensity was calculated. The MTV1 signal was quantified by measurement of the skewness of the signal distribution[23]. Images were analysed by means of Fiji[90], which was used to rotate and crop images.

Statistical analysis

All statistical analyses were done with the GraphPad Prism v.8 software. The rBiFC data statistics were done with Brown–Forsythe and Welch analysis of variance (ANOVA) tests with Dunnett T3 multiple comparisons. For the statistical analysis of the protein levels, two-way ANOVA was utilized and followed by Sidak multiple-comparisons test in the comparison procedure. The other multiple comparisons were done by one-way ANOVA with Dunnett's multiple-comparisons test.

Reporting summary

Further information on research design is available in the Nature Portfolio Reporting Summary linked to this article.

Data availability

The mass spectrometry proteomics data have been deposited to the ProteomeXchange Consortium via the PRIDE partner repository with the dataset identifier PXD035454 and 10.6019/PXD035454. Source data are provided with this paper.

References

1. Kirchhausen, T., Owen, D. & Harrison, S. C. Molecular structure, function, and dynamics of clathrin-mediated membrane traffic. *Cold Spring Harb. Perspect. Biol.* **6**, a016725 (2014).
2. Hirst, J. et al. The fifth adaptor protein complex. *PLoS Biol.* **9**, e1001170 (2011).
3. Sanger, A., Hirst, J., Davies, A. K. & Robinson, M. S. Adaptor protein complexes and disease at a glance. *J. Cell Sci.* **132**, jcs222992 (2019).
4. Aniento, F., Sánchez de Medina Hernández, V., Dagdas, Y., Rojas-Pierce, M. & Russinova, E. Molecular mechanisms of endomembrane trafficking in plants. *Plant Cell* **34**, 146–173 (2022).
5. Shimizu, Y. et al. Cargo sorting zones in the *trans*-Golgi network visualized by super-resolution confocal live imaging microscopy in plants. *Nat. Commun.* **12**, 1901 (2021).

6. Arora, D. & Van Damme, D. Motif-based endomembrane trafficking. *Plant Physiol.* **186**, 221–238 (2021).
7. Park, M. et al. *Arabidopsis* μ-adaptin subunit AP1M of adaptor protein complex 1 mediates late secretory and vacuolar traffic and is required for growth. *Proc. Natl Acad. Sci. USA* **110**, 10318–10323 (2013).
8. Teh, O.-K. et al. The AP-1 μ adaptin is required for KNOLLE localization at the cell plate to mediate cytokinesis in Arabidopsis. *Plant Cell Physiol.* **54**, 838–847 (2013).
9. Wang, J.-G. et al. HAPLESS13, the Arabidopsis *μ*1 adaptin, is essential for protein sorting at the trans-Golgi network/early endosome. *Plant Physiol.* **162**, 1897–1910 (2013).
10. Xu, M. et al. ADAPTOR PROTEIN-1 complex-mediated post-Golgi trafficking is critical for pollen wall development in Arabidopsis. *N. Phytol.* **235**, 472–487 (2022).
11. Kim, S. Y. et al. Adaptor protein complex 2-mediated endocytosis is crucial for male reproductive organ development in *Arabidopsis*. *Plant Cell* **25**, 2970–2985 (2013).
12. Di Rubbo, S. et al. The clathrin adaptor complex AP-2 mediates endocytosis of BRASSINOSTEROID INSENSITIVE1 in *Arabidopsis*. *Plant Cell* **25**, 2986–2997 (2013).
13. Liu, D. et al. Endocytosis of BRASSINOSTEROID INSENSITIVE1 is partly driven by a canonical Tyr-based motif. *Plant Cell* **32**, 3598–3612 (2020).
14. Yoshinari, A. et al. Polar localization of the borate exporter BOR1 requires AP2-dependent endocytosis. *Plant Physiol.* **179**, 1569–1580 (2019).
15. Fan, L. et al. Dynamic analysis of *Arabidopsis* AP2 σ subunit reveals a key role in clathrin-mediated endocytosis and plant development. *Development* **140**, 3826–3837 (2013).
16. Yamaoka, S. et al. Identification and dynamics of *Arabidopsis* adaptor protein-2 complex and its involvement in floral organ development. *Plant Cell* **25**, 2958–2969 (2013).
17. Feng, Q.-N., Liang, X., Li, S. & Zhang, Y. The ADAPTOR PROTEIN-3 complex mediates pollen tube growth by coordinating vacuolar targeting and organization. *Plant Physiol.* **177**, 216–225 (2018).
18. Feraru, E. et al. The AP-3 β adaptin mediates the biogenesis and function of lytic vacuoles in *Arabidopsis*. *Plant Cell* **22**, 2812–2824 (2010).
19. Wolfenstetter, S., Wirsching, P., Dotzauer, D., Schneider, S. & Sauer, N. Routes to the tonoplast: the sorting of tonoplast transporters in *Arabidopsis* mesophyll protoplasts. *Plant Cell* **24**, 215–232 (2012).
20. Zwiewka, M. et al. The AP-3 adaptor complex is required for vacuolar function in. *Arabidopsis. Cell Res.* **21**, 1711–1722 (2011).
21. Fuji, K. et al. The adaptor complex AP-4 regulates vacuolar protein sorting at the trans-Golgi network by interacting with VACUOLAR SORTING RECEPTOR1. *Plant Physiol.* **170**, 211–219 (2016).
22. Hatsugai, N. et al. Involvement of adapter protein complex 4 in hypersensitive cell death induced by avirulent bacteria. *Plant Physiol.* **176**, 1824–1834 (2017).
23. Heinze, L. et al. EPSIN1 and MTV1 define functionally overlapping but molecularly distinct *trans*-Golgi network subdomains in. *Arabidopsis. Proc. Natl Acad. Sci. USA* **117**, 25880–25889 (2020).
24. Pertl-Obermeyer, H. et al. Identification of cargo for adaptor protein (AP) complexes 3 and 4 by sucrose gradient profiling. *Mol. Cell. Proteom.* **15**, 2877–2889 (2016).
25. Gadeyne, A. et al. The TPLATE adaptor complex drives clathrin-mediated endocytosis in plants. *Cell* **156**, 691–704 (2014).
26. Johnson, A. et al. The TPLATE complex mediates membrane bending during plant clathrin-mediated endocytosis. *Proc. Natl Acad. Sci. USA* **118**, e2113046118 (2021).
27. Van Damme, D. et al. Somatic cytokinesis and pollen maturation in *Arabidopsis* depend on TPLATE, which has domains similar to coat proteins. *Plant Cell* **18**, 3502–3518 (2006).
28. Wang, J. et al. Conditional destabilization of the TPLATE complex impairs endocytic internalization. *Proc. Natl Acad. Sci. USA* **118**, e2023456118 (2021).
29. McMahon, H. T. & Boucrot, E. Molecular mechanism and physiological functions of clathrin-mediated endocytosis. *Nat. Rev. Mol. Cell Biol.* **12**, 517–533 (2011).
30. Merrifield, C. J. & Kaksonen, M. Endocytic accessory factors and regulation of clathrin-mediated endocytosis. *Cold Spring Harb. Perspect. Biol.* **6**, a016733 (2014).
31. Borner, G. H. H., Harbour, M., Hester, S., Lilley, K. S. & Robinson, M. S. Comparative proteomics of clathrin-coated vesicles. *J. Cell Biol.* **175**, 571–578 (2006).
32. Borner, G. H. H. et al. Multivariate proteomic profiling identifies novel accessory proteins of coated vesicles. *J. Cell Biol.* **197**, 141–160 (2012).
33. Praefcke, G. J. K. et al. Evolving nature of the AP2 α-appendage hub during clathrin-coated vesicle endocytosis. *EMBO J.* **23**, 4371–4383 (2004).
34. Schmid, E. M. et al. Role of the AP2 β-appendage hub in recruiting partners for clathrin-coated vesicle assembly. *PLoS Biol.* **4**, e262 (2006).
35. Dahhan, D. A. et al. Proteomic characterization of isolated Arabidopsis clathrin-coated vesicles reveals evolutionarily conserved and plant-specific components. *Plant Cell* **34**, 2150–2173 (2022).
36. Arora, D. et al. Establishment of proximity-dependent biotinylation approaches in different plant model systems. *Plant Cell* **32**, 3388–3407 (2020).
37. Adamowski, M. et al. A functional study of AUXILIN-LIKE1 and 2, two putative clathrin uncoating factors in Arabidopsis. *Plant Cell* **30**, 700–716 (2018).
38. Zhang, L. et al. SNARE proteins VAMP721 and VAMP722 mediate the post-Golgi trafficking required for auxin-mediated development in Arabidopsis. *Plant J.* **108**, 426–440 (2021).
39. Zouhar, J. & Sauer, M. Helping hands for budding prospects: ENTH/ANTH/VHS accessory proteins in endocytosis, vacuolar transport, and secretion. *Plant Cell* **26**, 4232–4244 (2014).
40. Ritter, B. et al. NECAP 1 regulates AP-2 interactions to control vesicle size, number, and cargo during clathrin-mediated endocytosis. *PLoS Biol.* **11**, e1001670 (2013).
41. Kabbage, M., Kessens, R., Bartholomay, L. C. & Williams, B. The life and death of a plant cell. *Annu. Rev. Plant Biol.* **68**, 375–404 (2017).
42. Gulbranson, D. R. et al. AAGAB controls AP2 adaptor assembly in clathrin-mediated endocytosis. *Dev. Cell* **50**, 436–446 (2019).
43. Pohler, E. et al. Haploinsufficiency for *AAGAB* causes clinically heterogeneous forms of punctate palmoplantar keratoderma. *Nat. Genet.* **44**, 1272–1276 (2012).
44. Conner, S. D. & Schmid, S. L. Identification of an adaptor-associated kinase, AAK1, as a regulator of clathrin-mediated endocytosis. *J. Cell Biol.* **156**, 921–929 (2002).
45. Agajanian, M. J. et al. WNT activates the AAK1 kinase to promote clathrin-mediated endocytosis of LRP6 and establish a negative feedback loop. *Cell Rep.* **26**, 79–93 (2019).
46. Hirst, J. et al. Interaction between AP-5 and the hereditary spastic paraplegia proteins SPG11 and SPG15. *Mol. Biol. Cell* **24**, 2558–2569 (2013).
47. Zhuang, X. et al. A BAR-domain protein SH3P2, which binds to phosphatidylinositol 3-phosphate and ATG8, regulates autophagosome formation in *Arabidopsis*. *Plant Cell* **25**, 4596–4615 (2013).
48. Lam, B. C., Sage, T. L., Bianchi, F. & Blumwald, E. Regulation of ADL6 activity by its associated molecular network. *Plant J.* **31**, 565–576 (2002).

49. Lauber, M. H. et al. The *Arabidopsis* KNOLLE protein is a cytokinesis-specific syntaxin. *J. Cell Biol.* **139**, 1485–1493 (1997).
50. Favery, B. et al. Arabidopsis formin AtFH6 is a plasma membrane–associated protein upregulated in giant cells induced by parasitic nematodes. *Plant Cell* **16**, 2529–2540 (2004).
51. Blomme, J. et al. The heat is on: a simple method to increase genome editing efficiency in plants. *BMC Plant Biol.* **22**, 142 (2022).
52. Yan, X. et al. Cross-talk between clathrin-dependent post-Golgi trafficking and clathrin-mediated endocytosis in Arabidopsis root cells. *Plant Cell* **33**, 3057–3075 (2021).
53. Samalova, M., Fricker, M. & Moore, I. Ratiometric fluorescence-imaging assays of plant membrane traffic using polyproteins. *Traffic* **7**, 1701–1723 (2006).
54. Reichardt, I. et al. Plant cytokinesis requires de novo secretory trafficking but not endocytosis. *Curr. Biol.* **17**, 2047–2053 (2007).
55. Boutté, Y. et al. Endocytosis restricts *Arabidopsis* KNOLLE syntaxin to the cell division plane during late cytokinesis. *EMBO J.* **29**, 546–558 (2010).
56. Law, K. C., Chung, K. K. & Zhuang, X. An update on coat protein complexes for vesicle formation in plant post-Golgi trafficking. *Front. Plant Sci.* **13**, 826007 (2022).
57. Van Leene, J. et al. An improved toolbox to unravel the plant cellular machinery by tandem affinity purification of *Arabidopsis* protein complexes. *Nat. Protoc.* **10**, 169–187 (2015).
58. Peden, A. A., Rudge, R. E., Lui, W. W. Y. & Robinson, M. S. Assembly and function of AP-3 complexes in cells expressing mutant subunits. *J. Cell Biol.* **156**, 327–336 (2002).
59. Rout, M. P. & Field, M. C. The evolution of organellar coat complexes and organization of the eukaryotic cell. *Annu. Rev. Biochem.* **86**, 637–657 (2017).
60. Ricotta, D., Conner, S. D., Schmid, S. L., von Figura, K. & Höning, S. Phosphorylation of the AP2 μ subunit by AAK1 mediates high affinity binding to membrane protein sorting signals. *J. Cell Biol.* **156**, 791–795 (2002).
61. Gupta-Rossi, N. et al. The adaptor-associated kinase 1, AAK1, is a positive regulator of the Notch pathway. *J. Biol. Chem.* **286**, 18720–18730 (2011).
62. Behl, C. & Breaking, B. A. G. the co-chaperone BAG3 in health and disease. *Trends Pharmacol. Sci.* **37**, 672–688 (2016).
63. Korbei, B. et al. Arabidopsis TOL proteins act as gatekeepers for vacuolar sorting of PIN2 plasma membrane protein. *Curr. Biol.* **23**, 2500–2505 (2013).
64. Moulinier-Anzola, J. et al. TOLs function as ubiquitin receptors in the early steps of the ESCRT pathway in higher plants. *Mol. Plant* **13**, 717–731 (2020).
65. Wang, P. et al. Plant AtEH/Pan1 proteins drive autophagosome formation at ER-PM contact sites with actin and endocytic machinery. *Nat. Commun.* **10**, 5132 (2019).
66. Adamowski, M., Matijevic, I. & Friml, J. The role of clathrin in exocytosis and the mutual regulation of endo- and exocytosis in plant cells. Preprint at *bioRxiv* https://doi.org/10.1101/2021.11.17.468992 (2021).
67. Van Damme, D. et al. Adaptin-like protein TPLATE and clathrin recruitment during plant somatic cytokinesis occurs via two distinct pathways. *Proc. Natl Acad. Sci. USA* **108**, 615–620 (2011).
68. Zhang, C. et al. ROPGAP-dependent interaction between brassinosteroid and ROP2-GTPase signaling controls pavement cell shape in. *Arabidopsis. Curr. Biol.* **32**, 518–531 (2022).
69. Shimada, T. et al. The AP-1 complex is required for proper mucilage formation in Arabidopsis seeds. *Plant Cell Physiol.* **59**, 2331–2338 (2018).
70. Müdsam, C., Wollschläger, P., Sauer, N. & Schneider, S. Sorting of *Arabidopsis* NRAMP3 and NRAMP4 depends on adaptor protein complex AP4 and a dileucine-based motif. *Traffic* **19**, 503–521 (2018).
71. Robert, S. et al. Endosidin1 defines a compartment involved in endocytosis of the brassinosteroid receptor BRI1 and the auxin transporters PIN2 and AUX1. *Proc. Natl Acad. Sci. USA* **105**, 8464–8469 (2008).
72. Dettmer, J., Hong-Hermesdorf, A., Stierhof, Y.-D. & Schumacher, K. Vacuolar H^+-ATPase activity is required for endocytic and secretory trafficking in *Arabidopsis*. *Plant Cell* **18**, 715–730 (2006).
73. Karimi, M., Inzé, D. & Depicker, A. GATEWAY™ vectors for *Agrobacterium*-mediated plant transformation. *Trends Plant Sci.* **7**, 193–195 (2002).
74. Decaestecker, W. et al. CRISPR-TSKO: a technique for efficient mutagenesis in specific cell types, tissues, or organs in Arabidopsis. *Plant Cell* **31**, 2868–2887 (2019).
75. Stemmer, M., Thumberger, T., del Sol Keyer, M., Wittbrodt, J. & Mateo, J. L. CCTop: an intuitive, flexible and reliable CRISPR/Cas9 target prediction tool. *PLoS ONE* **10**, e0124633 (2015).
76. Houbaert, A. et al. POLAR-guided signalling complex assembly and localization drive asymmetric cell division. *Nature* **563**, 574–578 (2018).
77. Hu, Z. et al. Genome editing-based engineering of CESA3 dual cellulose-inhibitor-resistant plants. *Plant Physiol.* **180**, 827–836 (2019).
78. Grefen, C. & Blatt, M. R. A 2in1 cloning system enables ratiometric bimolecular fluorescence complementation (rBiFC). *Biotechniques* **53**, 311–314 (2012).
79. Knight, J. D. R. et al. ProHits-viz: a suite of web tools for visualizing interaction proteomics data. *Nat. Methods* **14**, 645–646 (2017).
80. Ge, S. X., Jung, D. & Yao, R. ShinyGO: a graphical gene-set enrichment tool for animals and plants. *Bioinformatics* **36**, 2628–2629 (2020).
81. Sauer, M., Paciorek, T., Benková, E. & Friml, J. Immunocytochemical techniques for whole-mount in situ protein localization in plants. *Nat. Protoc.* **1**, 98–103 (2006).
82. Abas, L. et al. Intracellular trafficking and proteolysis of the *Arabidopsis* auxin-efflux facilitator PIN2 are involved in root gravitropism. *Nat. Cell Biol.* **8**, 249–256 (2006).
83. Feng, J. & Ma, L. A method for characterizing embryogenesis in. *Arabidopsis. JoVE* **126**, e55969 (2017).
84. Zhai, Z., Jung, H.-I. & Vatamaniuk, O. K. Isolation of protoplasts from tissues of 14-day-old seedlings of *Arabidopsis thaliana*. *JoVE* **30**, e1149 (2009).
85. Wang, C. et al. Differential regulation of clathrin and its adaptor proteins during membrane recruitment for endocytosis. *Plant Physiol.* **171**, 215–229 (2016).
86. Song, K. et al. An A/ENTH domain-containing protein functions as an adaptor for clathrin-coated vesicles on the growing cell plate in Arabidopsis root cells. *Plant Physiol.* **159**, 1013–1025 (2012).
87. Kim, Y.-W. et al. Arabidopsis dynamin-like 2 that binds specifically to phosphatidylinositol 4-phosphate assembles into a high-molecular weight complex in vivo and in vitro. *Plant Physiol.* **127**, 1243–1255 (2001).
88. Dejonghe, W. et al. Disruption of endocytosis through chemical inhibition of clathrin heavy chain function. *Nat. Chem. Biol.* **15**, 641–649 (2019).
89. Luo, Y. et al. V-ATPase activity in the TGN/EE is required for exocytosis and recycling in *Arabidopsis*. *Nat. Plants* **1**, 15094 (2015).
90. Schindelin, J., Rueden, C. T., Hiner, M. C. & Eliceiri, K. W. The ImageJ ecosystem: an open platform for biomedical image analysis. *Mol. Reprod. Dev.* **82**, 518–529 (2015).

Acknowledgements

We thank I. Hwang, G. Jürgens and J. Pan for the kind gift of α-AP1G and α-AP2A, α-KNOLLE and α-AP2S antibodies, respectively, M. Sauer, S. Schneider, J. Friml, J. Lin and I. Hara-Nishimura for providing published

materials, T. Jacobs for useful discussions and M. De Cock for help in preparing the manuscript. This work was supported by the Research Foundation-Flanders projects (G008416N, G0E5718N and 3G038020 to E.R.), the Belgian Science Policy Office for a postdoctoral fellowship (R.K.), the China Scholarship Council for predoctoral fellowships (P.W., X.Z. and R.W.) and the European Research Council T-Rex (project number 682436 to D.V.D.).

Author contributions

W.S., P.W., X.Z. and E.R. initiated the project and designed experiments. W.S., X.Z., R.K., A.H. and N.D.W. did cloning for TAP–MS and AP–MS. D.E., J.V.L., K.G. and G.D.J. performed the MS work and analysed data. W.S. and P.W. did the interactome validation. P.W. performed all the P34 work. E.M. did microscopy. R.A.K. and C.T. contributed materials. D.A., M.V. and D.V.D. did the PL. R.W. and S.V. performed the PIN2 immunolabelling. W.S., P.W. and E.R. wrote the manuscript. All authors revised the manuscript.

Competing interests

The authors declare no competing interests.

Additional information

Extended data is available for this paper at https://doi.org/10.1038/s41477-022-01328-2.

Supplementary information The online version contains supplementary material available at https://doi.org/10.1038/s41477-022-01328-2.

Correspondence and requests for materials should be addressed to Wei Siao or Eugenia Russinova.

Peer review information *Nature Plants* thanks Takashi Ueda, Michael Sauer and the other, anonymous, reviewer(s) for their contribution to the peer review of this work.

Reprints and permissions information is available at www.nature.com/reprints.

Publisher's note Springer Nature remains neutral with regard to jurisdictional claims in published maps and institutional affiliations.

Springer Nature or its licensor (e.g. a society or other partner) holds exclusive rights to this article under a publishing agreement with the author(s) or other rightsholder(s); author self-archiving of the accepted manuscript version of this article is solely governed by the terms of such publishing agreement and applicable law.

© The Author(s), under exclusive licence to Springer Nature Limited 2023

https://doi.org/10.1038/s41477-022-01328-2

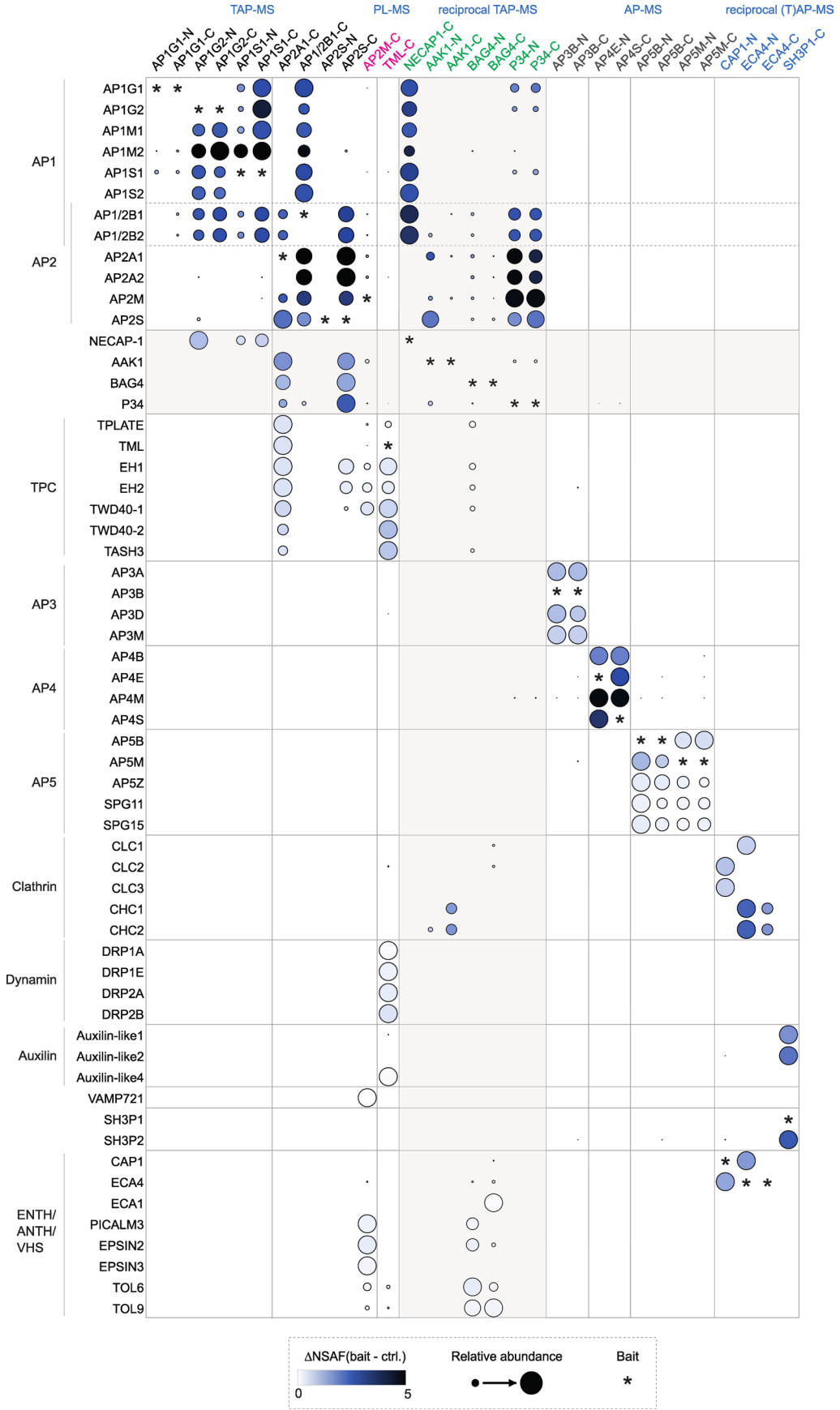

Extended Data Fig. 1 | Dot plot matrix of selected proteins from the AP/TPC interactome. Quantitative dot plot matrix covering core AP/TPC subunits and a selection of proteins linked to endocytosis/vesicle trafficking. The colour hue of the nodes corresponds with the abundance of each prey in a given experiment, calculated by subtracting the average normalized spectral abundance factor (NSAF) in the control dataset from the average NSAF (bait) of each prey [NSAF (bait - ctrl.)]. The size of the dots reflects the relative abundance of each prey over the different experiments. The identification of each bait protein is shown by an asterisk.

https://doi.org/10.1038/s41477-022-01328-2

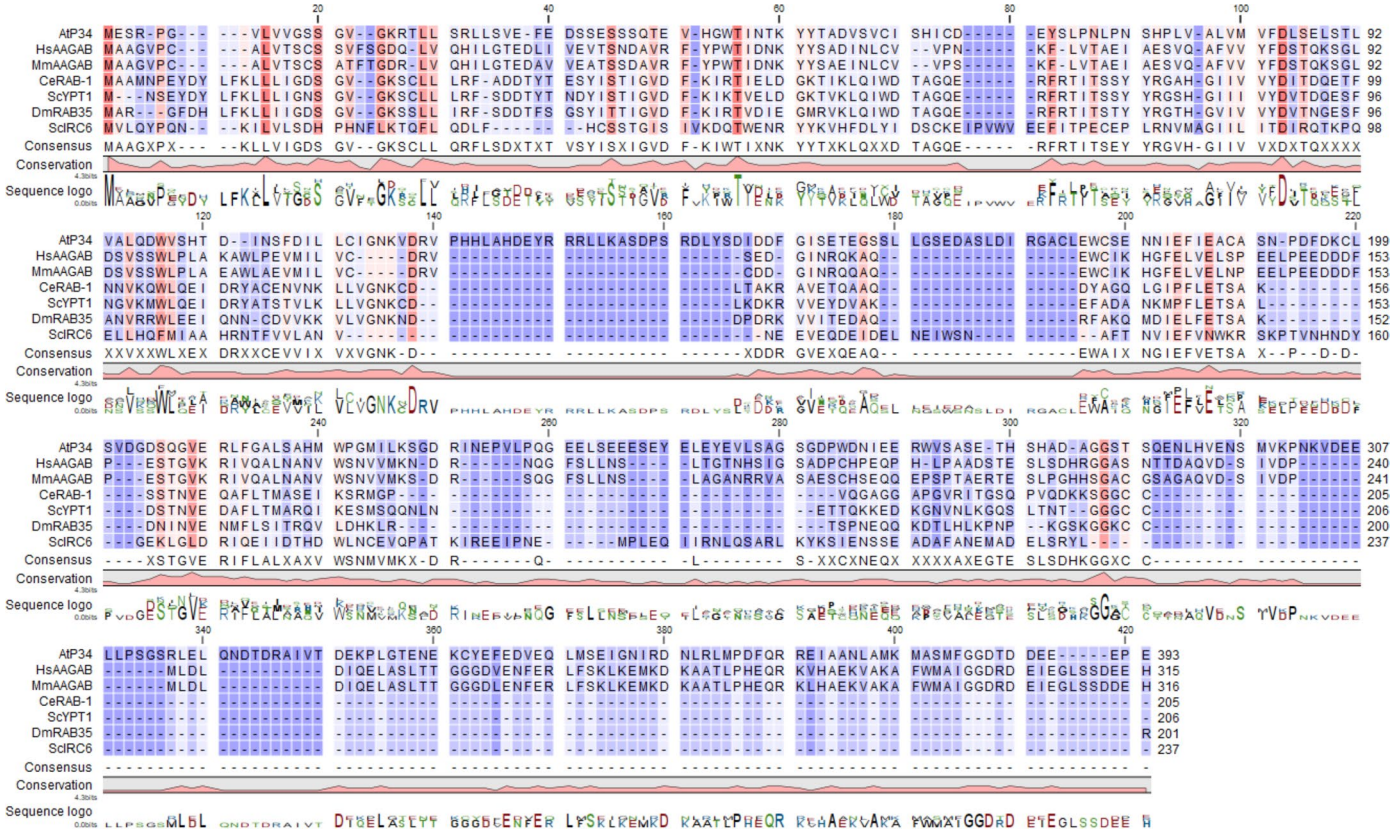

Extended Data Fig. 2 | Protein sequence alignment of P34 in eukaryotes. Amino acid sequence alignment of the P34/AAGAB family in At, *Arabidopsis thaliana*; Hs, *Homo sapiens*; Mm, *Mus musculus*; Ce, *Caenorhabditis elegans*; Sc, *Saccharomyces cerevisiae*; Dm, *Drosophila melanogaster*. The sequences were aligned with the CLC Main Workbench (Qiagen). The colour intensity reflects how conserved a particular position is in the alignment. Dark orange and dark purple represents 100% and 0% identity, respectively.

https://doi.org/10.1038/s41477-022-01328-2

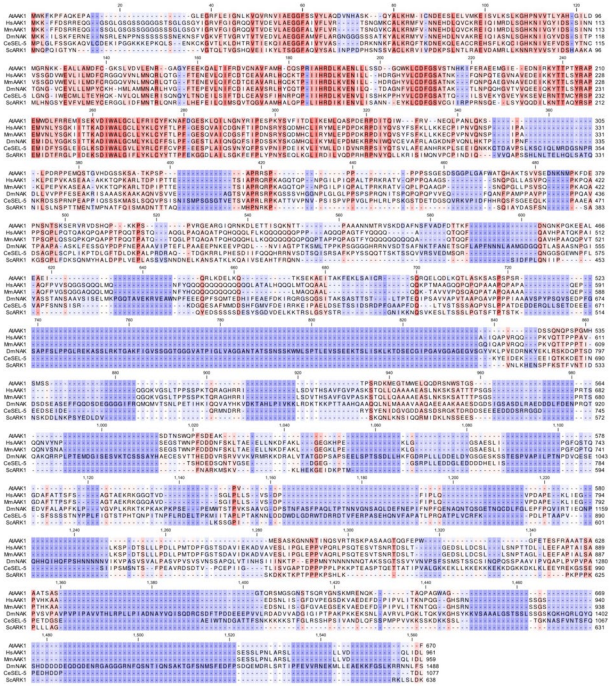

Extended Data Fig. 3 | Protein sequence alignment of AAK1 in eukaryotes. Amino acid sequence alignment of the NAK family in At, *Arabidopsis thaliana*; Hs, *Homo sapiens*; Mm, *Mus musculus*; Dm, *Drosophila melanogaster*; Ce, *Caenorhabditis elegans*, and Sc, *Saccharomyces cerevisiae*. The sequences were aligned with CLC Main Workbench (Qiagen). The colour intensity reflects how conserved the particular position is in the alignment. Dark orange and dark purple represent 100% and 0% identity, respectively.

https://doi.org/10.1038/s41477-022-01328-2

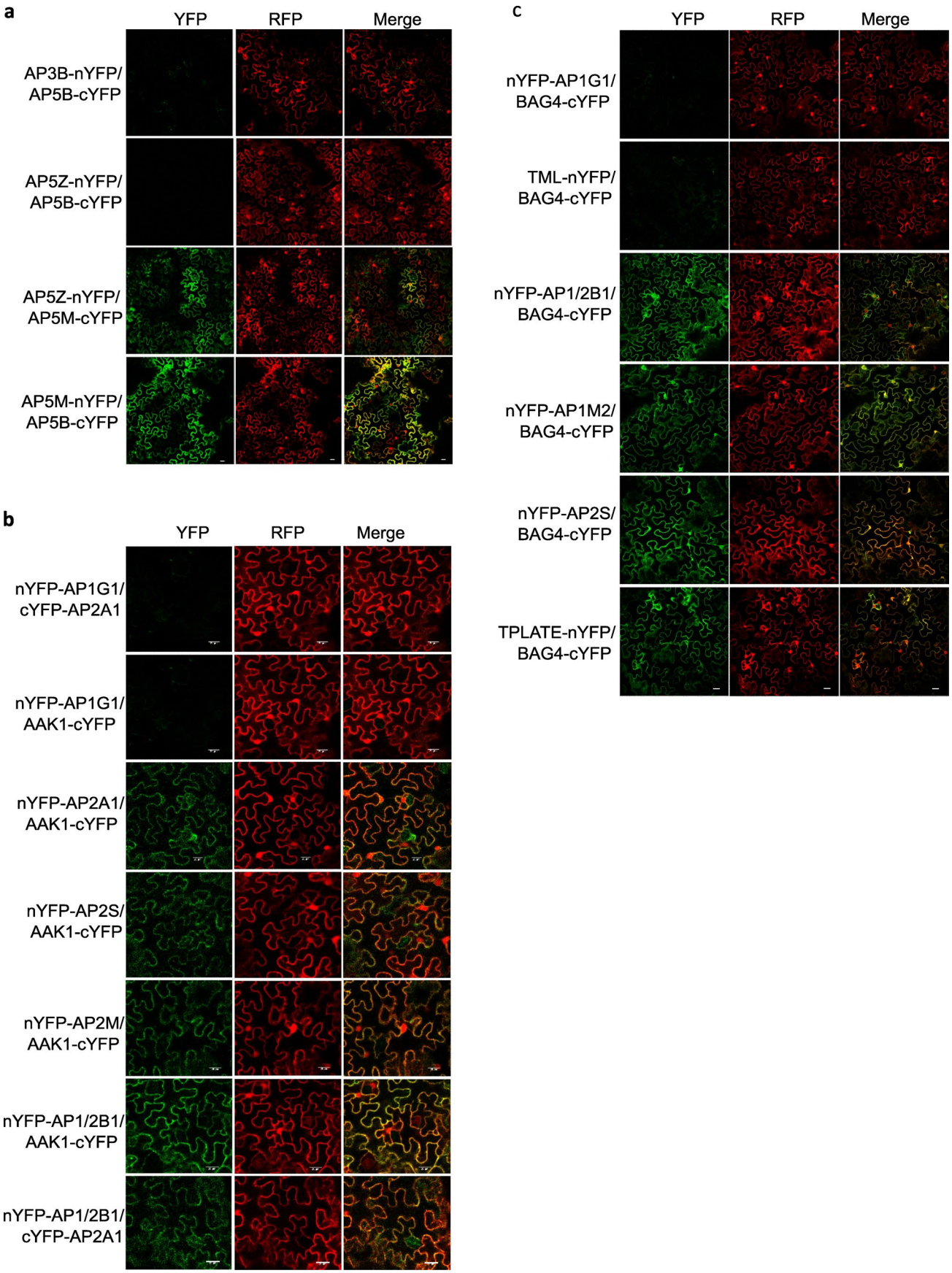

Extended Data Fig. 4 | rBiFC analysis of AP-5, AAK1 and BAG4. rBiFC assay of AP-5 subunits (**a**), AAK1 (**b**) and BAG4 (**c**) with different AP subunits quantified in Fig. 4b,e,h, respectively. Scale bars, 20 μm.

https://doi.org/10.1038/s41477-022-01328-2

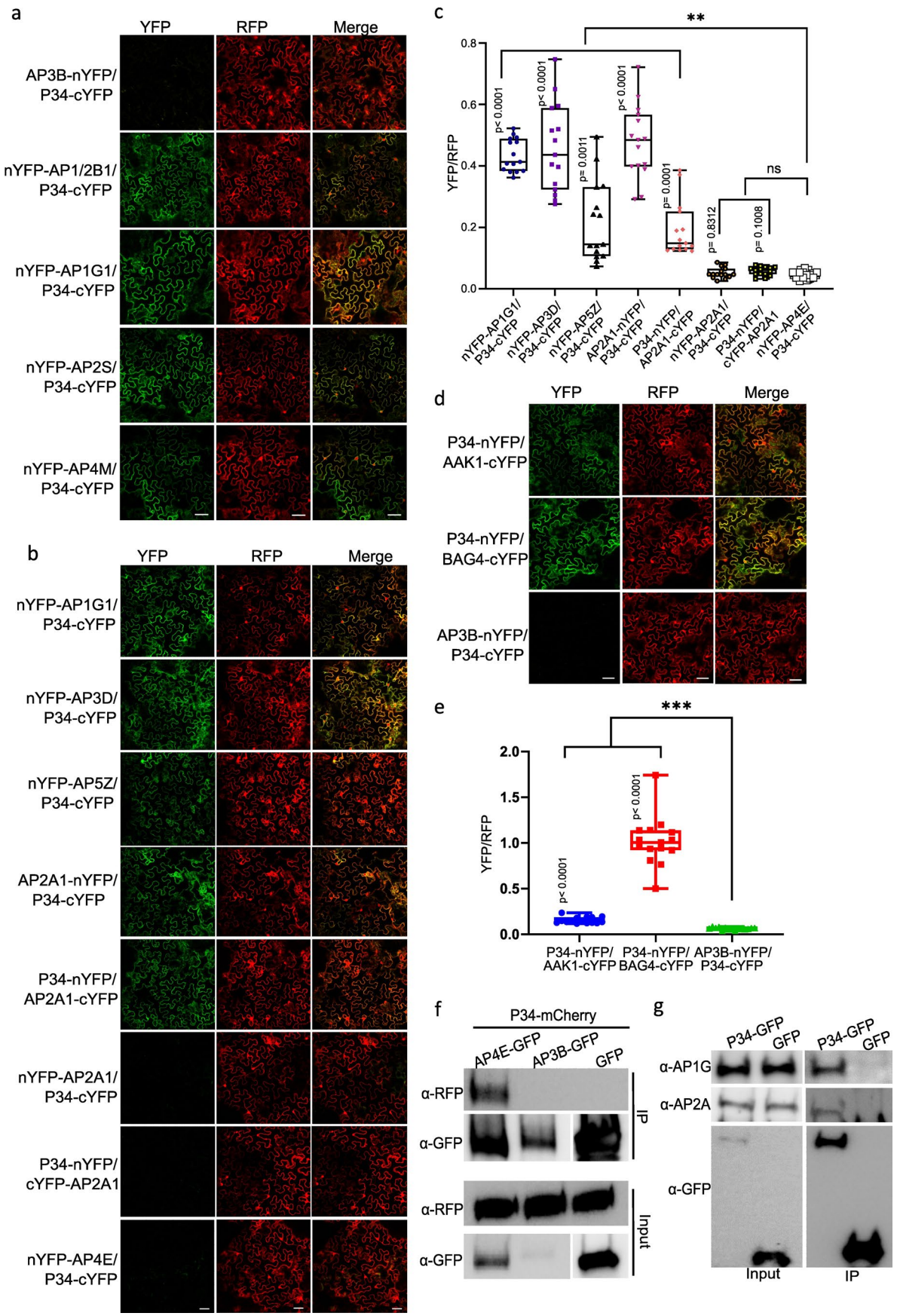

Extended Data Fig. 5 | See next page for caption.

https://doi.org/10.1038/s41477-022-01328-2

Extended Data Fig. 5 | rBiFC and co-immunoprecipitation (co-IP) analyses of P34. rBiFC assays of P34 with different AP subunits (quantified in Fig. 4k) (**a**,**b**), with AAK1 and BAG4 (**d**). **c**,**e**, Quantification of rBiFC (YFP/RFP) in (**b**) and (**d**), respectively. $n = 15$, n, number of cells analysed. The significant differences were determined by one way Brown-Forsythe and Welch ANOVA tests combined with Dunnett T3 multiple comparisons test. $^{**}P \leq 0.01$, $^{***}P \leq 0.001$; ns, not significant. The bounds of the boxes represent the 25th to 75th percentiles, the center line of the box and the whiskers indicate the median, the minimum and the maximum values, respectively. All individual values were plotted. rBiFC experiments were repeated twice and one representative experiment is shown. Scale bars, 50 µm. **f**, Validation of the interactions between P34, AP3B, and AP4E by co-IP in tobacco leaves transiently expressing the *p35S:P34-mCherry*, *p35S:AP3B-GFP* and *p35S:AP4E-GFP* constructs. **g**, co-IP analysis in *ap4m-2* protoplasts transiently expressing *p35S:P34-GFP*. P34-GFP was pulled down with a GFP-trap and AP1G and AP2A were detected with the α-AP1G and α-AP2A antibodies. The *p35S:GFP* construct was used as a negative control (**f**,**g**), The two western blots were repeated two times. One representative experiment is shown.

https://doi.org/10.1038/s41477-022-01328-2

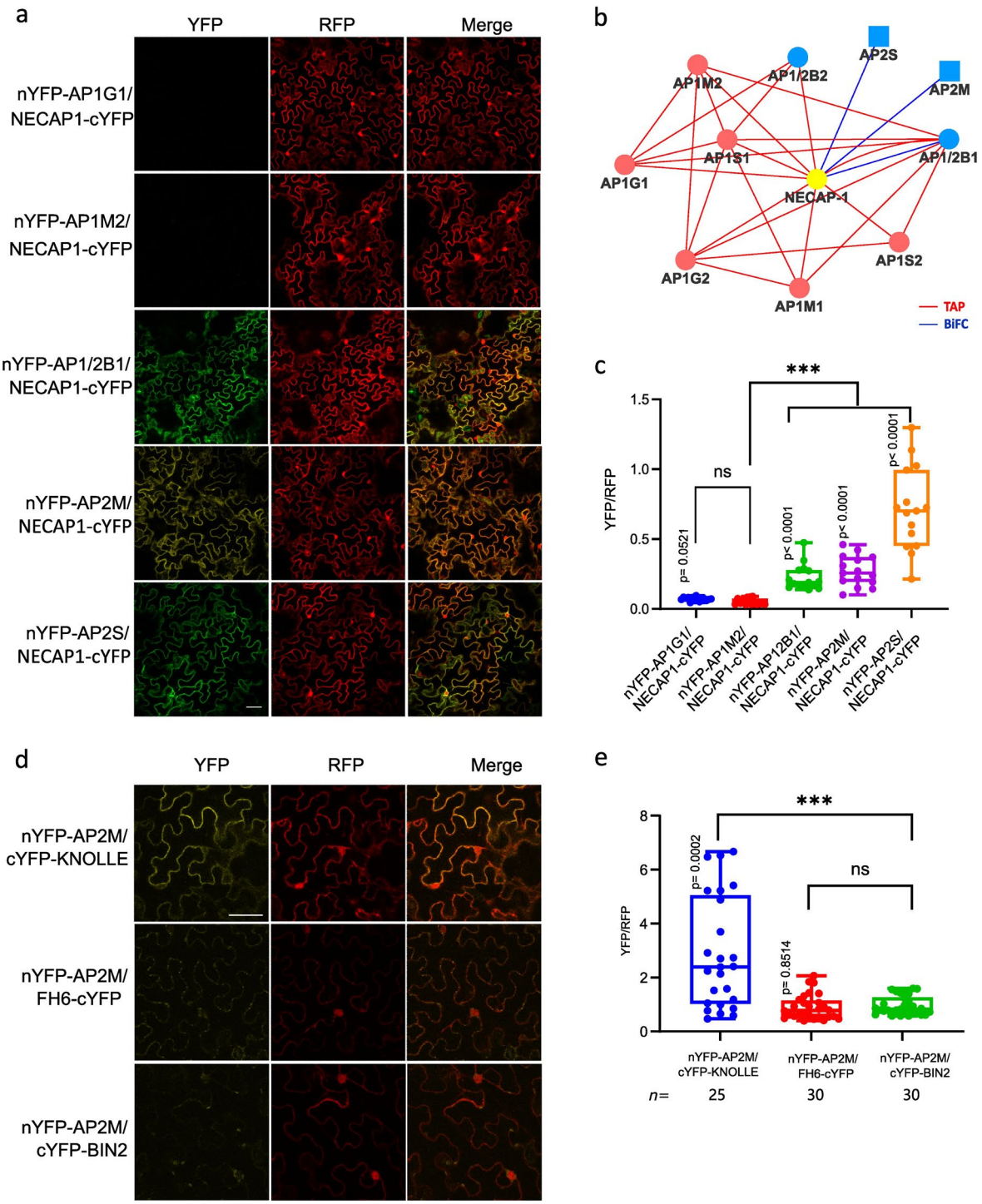

Extended Data Fig. 6 | BiFC analysis of NECAP-1 and the putative AP2M cargos discovered by PL-MS. a, rBiFC assay of NECAP-1 with different AP-1 and AP-2 subunits. Scale bars, 50 µm. **b**, Cytoscape model summarizing the interactions between various subunits and NECAP-1. Edge colours indicate the analysis method. Node colours correspond to the different complexes and protein families, red and blue, for AP-1 and AP-2, respectively. **c**, Quantification of rBiFC (YFP/RFP) in (**a**). rBiFC experiments were repeated twice and one representative experiment is shown. $n = 15$. **d**, rBIFC assay of AP2M interaction with KNOLLE and FORMIN-LIKE PROTEIN 6 (FH6), observed by PL-MS with AP2M as bait. The SHAGGY-like kinase BIN2 was used as negative control. Whereas AP2M interacts with KNOLLE evenly along the plasma membrane, the interaction between AP2M and FH6 is less intense and concentrated in plasma membrane-associated punctate. AP2M and BIN2 do not visually interact and only background and chlorophyll fluorescence are observed. **e**, Quantification of rBiFC (YFP/RFP PM intensity ratio) in (**d**) clearly shows significant differences between AP2M-KNOLLE and AP2M-BIN2. The punctate signal in the AP2M-FH6 combination is not sufficiently strong to yield a statistical difference compared to the control. *n*, number of cells analysed (**c**,**e**). The significant differences (**c**,**e**) were determined by one way Brown-Forsythe and Welch ANOVA tests with Dunnett T3 multiple comparisons test. ***$P < 0.001$; ns, not significant. The bounds of the boxes represent the 25th to 75th percentiles, the center line of the box indicates and the whiskers indicate the median, the minimum and the maximum values, respectively. All individual values were plotted. Scale bar, 50 µm.

https://doi.org/10.1038/s41477-022-01328-2

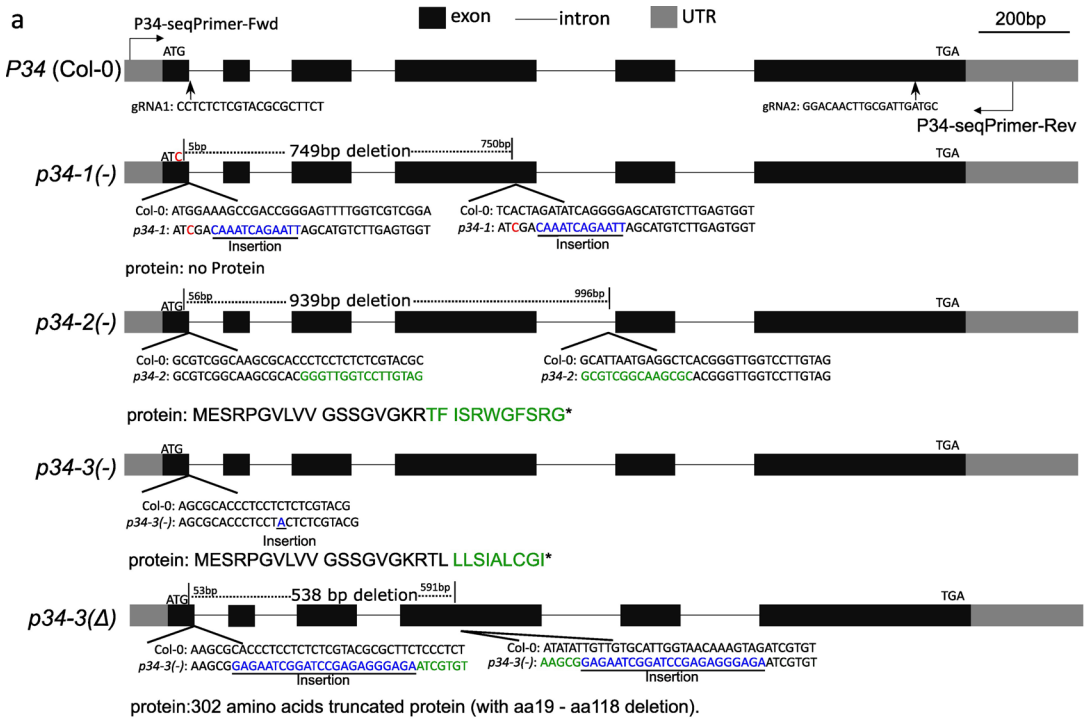

b

```
P34(Col-0) ME SRPGVLVV GS SGVGKRTL LSRLLSVEFE DSSESSSQTE VHGWTINTKY YTADVSVCIS 60
P34-3(Δ)   ME SRPGVLVV GS SGVGKRRI --------GSERE ---------- ---------- ---------- 25

P34(Col-0) HICD EYSLPN LPNSHPLVAL VMV FDLSELS TLVALQDWVS HTDINSFDIL LCIGN KVDRV 120
P34-3(Δ)   ---------- ---------- ---------- ---------- ---------- ----------NRV 28

P34(Col-0) PHH LAHD EYR RR LLKASDPS RD LYSDIDD F GISETEGS SL LGS EDASLDI RG AC LEWCSE 180
P34-3(Δ)   PHH LAHD EYR RR LLKASDPS RD LYSDIDD F GISETEGS SL LGS EDASLDI RG AC LEWCSE 88

P34(Col-0) NN IEFIEAC A SNPDFDKCLS VDGD SQG VER LFGALSAHMW PGM ILKSGDR INEPVLPQGE 240
P34-3(Δ)   NN IEFIEAC A SNPDFDKCLS VDGD SQG VER LFGALSAHMW PGM ILKSGDR INEPVLPQGE 148

P34(Col-0) ELSEEESEYE LEYEVLSAGS GD PWDN IEER WVSASETHSH AD AGGSTSQE NLHVENSMVK 300
P34-3(Δ)   ELSEEESEYE LEYEVLSAGS GD PWDN IEER WVSASETHSH AD AGGSTSQE NLHVENSMVK 208

P34(Col-0) PNKVD EELLP SGS RLELQND TDRAIVTDEK PLGTENEKCY EFEDVEQLMS EIGN IRDN LR 360
P34-3(Δ)   PNKVD EELLP SGS RLELQND TDRAIVTDEK PLGTENEKCY EFEDVEQLMS EIGN IRDN LR 268

P34(Col-0) LMPDFQRR EI AAN LAMKMAS MFGGDTDDEE EPE* 394
P34-3(Δ)   LMPDFQRR EI AAN LAMKMAS MFGGDTDDEE EPE* 302
```

Extended Data Fig. 7 | Genotype of the *P34-CRISPR* lines. a, Schematic representation of the CRISPR editing on the *P34* gene in the *p34* CRISPR mutants. Blue, red, and green indicate insertion, nucleotide exchange, and mutated amino acids, respectively. The arrows mark the sites of the guide RNA (gRNA) sequences. **b**, Protein sequence alignment of P34 (wild type, Col-0) and P34(Δ) by means of the CLC Main Workbench (Qiagen). Hyphen and green letters indicate deletion and mutated amino acids, respectively. Asterisks mark the stop codons.

https://doi.org/10.1038/s41477-022-01328-2

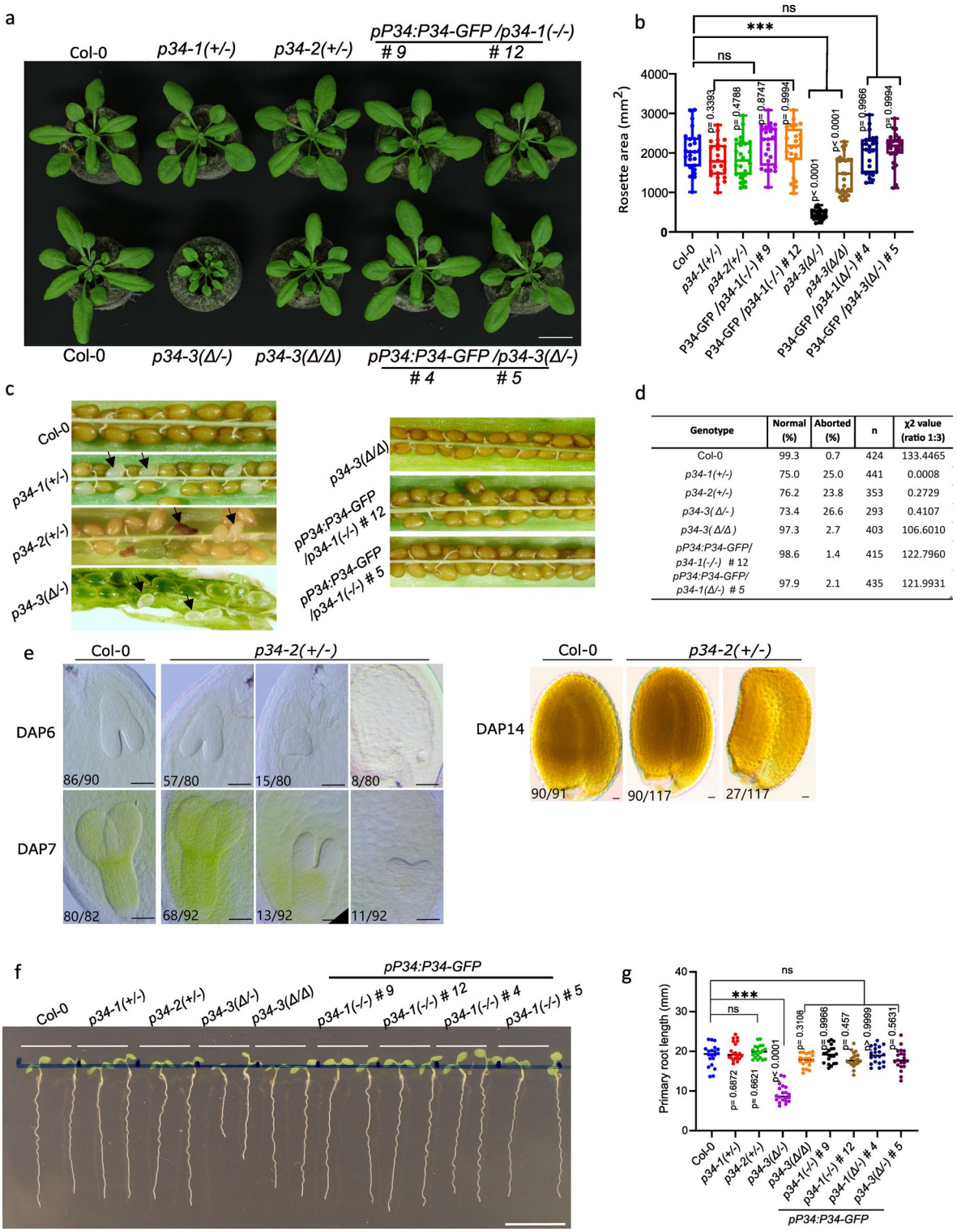

Genotype	Normal (%)	Aborted (%)	n	χ2 value (ratio 1:3)
Col-0	99.3	0.7	424	133.4465
p34-1(+/-)	75.0	25.0	441	0.0008
p34-2(+/-)	76.2	23.8	353	0.2729
p34-3(Δ/-)	73.4	26.6	293	0.4107
p34-3(Δ/Δ)	97.3	2.7	403	106.6010
pP34:P34-GFP/ p34-1(-/-) # 12	98.6	1.4	415	122.7960
pP34:P34-GFP/ p34-1(Δ/-) # 5	97.9	2.1	435	121.9931

Extended Data Fig. 8 | Phenotype of the *P34-CRISPR* lines. a, Rosettes of wild type (Col-0), *p34-1(+/-)*, *p34-2(+/-)*, *p34-3(Δ/-)*, *p34-3(Δ/Δ)* mutants, and *p34-1(-/-)* (lines #9 and #12) and *p34-3(Δ/-)* (lines #4 and #5) mutants complemented with the *pP34:gP34-GFP* construct grown in the soil for 4 weeks. Scale bar, 20 mm. **b**, Quantification the rosette leaf area of each genotype show in (**a**). Three independent experiments were combined, each with 8-9 plants per genotype. ***$P \leq 0.001$ (one-way ANOVA test); ns, not significant. The bounds of the boxes represent the 25th to 75th percentiles, the center line of the box and the whiskers indicate the median, the minimum and the maximum values, respectively. All individual values were plotted. **c**, Aborted seeds in the siliques of genotypes in (**b**). Arrows indicate the aborted seeds. **d**, Quantification of the aborted seeds in (**c**). χ^2 values were calculated with the χ^2 test. *n* number of seeds analysed. **e**, Embryogenesis of the wild type and the *p34-2(+/-)* mutant. Differential interference contrast (DIC) microscopy of cleared whole-mount seeds at 6, 7 and 14 DAP (days after pollination). The ratio indicates the ratio of observed embryo stage/total embryos. Scale bars, 20 µm. The quantification data are combined from two experiments. Representative images from one experiment are shown. **f**, Phenotype of 7-day-old seedlings grown on ½MS. Scale bar, 10 mm. **g**, Primary root length of seedlings shown in (**f**). All the individual values were plotted and the center line represents the median. Twenty roots per genotype were measured. ***$P \leq 0.001$ (one-way ANOVA test).

https://doi.org/10.1038/s41477-022-01328-2

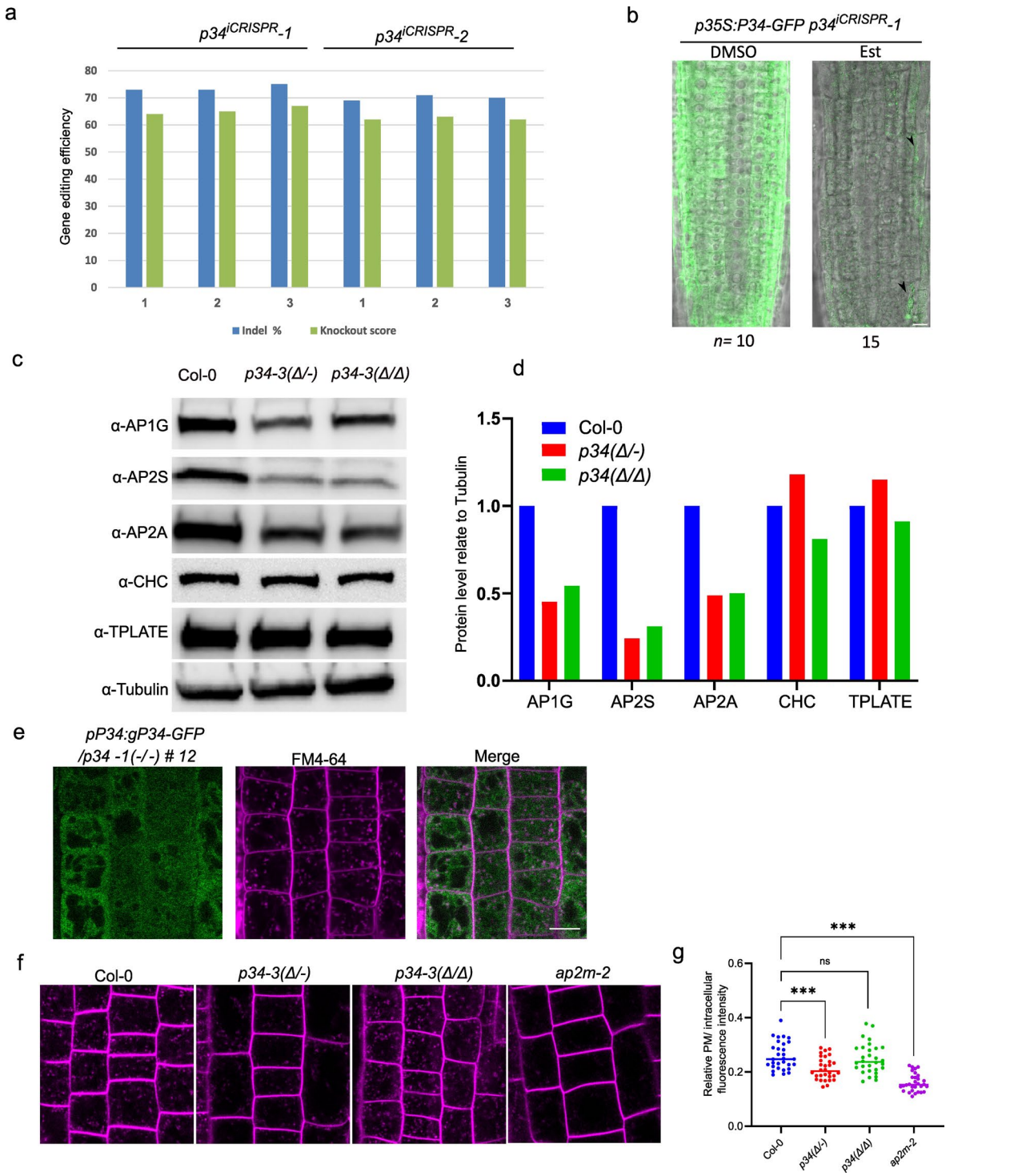

Extended Data Fig. 9 | CRISPR efficiency and different phenotypes of the *p34* mutants. a, Gene editing efficiency analysis of three random 9-day-old plants of *p34*^{iCRISPR}*-1* and *p34*^{iCRISPR}*-2* after induction with 10 μM β-oestradiol (Est). The sequencing results were analysed with the online software Inference of CRISPR Edits (ICE) (https://ice.synthego.com/#/). **b**, P34-GFP localization in roots of 5-day-old *p35S:gP34-GFP/p34*^{iCRISPR}*-1* plants grown on DMSO and 10 μM Est. Arrows indicate the remaining P34-GFP signal. Scale bar, 10 μm. **c**, Protein levels of AP1G, AP2A and AP2S in *p34-3* mutants analysed by immunoblotting with α-AP1G, α-AP2S, α-AP2A, α-CHC, α-TPLATE and α-Tubulin, The experiments were repeated three times. One representative experiment is shown. **d**, Quantification of protein levels shown in (**c**). The protein level was normalized to tubulin. **e**, Confocal images of the 5-day-old *pP34:gP34-GFP/p34-1(-/-)* (line #12) root cells stained with FM4-64 (2 μM, 40 min). Scale bar, 10 μm. The imaging was repeated three times. One representative experiment is shown. **f**, FM4-64 uptake in the *p34-3* mutants. **g**, Fluorescence intensity ratio of the relative intracellular-to-plasma membrane (PM) FM4-64 signal. All the individual value were plotted and the center line represents the median. ***$P \leq 0.001$ (one-way ANOVA test); ns, not significant. The P values versus the Col-0 control for *p34(Δ/-)* = 0.0004, *p34(Δ/Δ)* = 0.6980 and *ap2m-2* < 0.0001. $n = 30$, n number of cells analysed, Scale bar, 10 μm.

https://doi.org/10.1038/s41477-022-01328-2

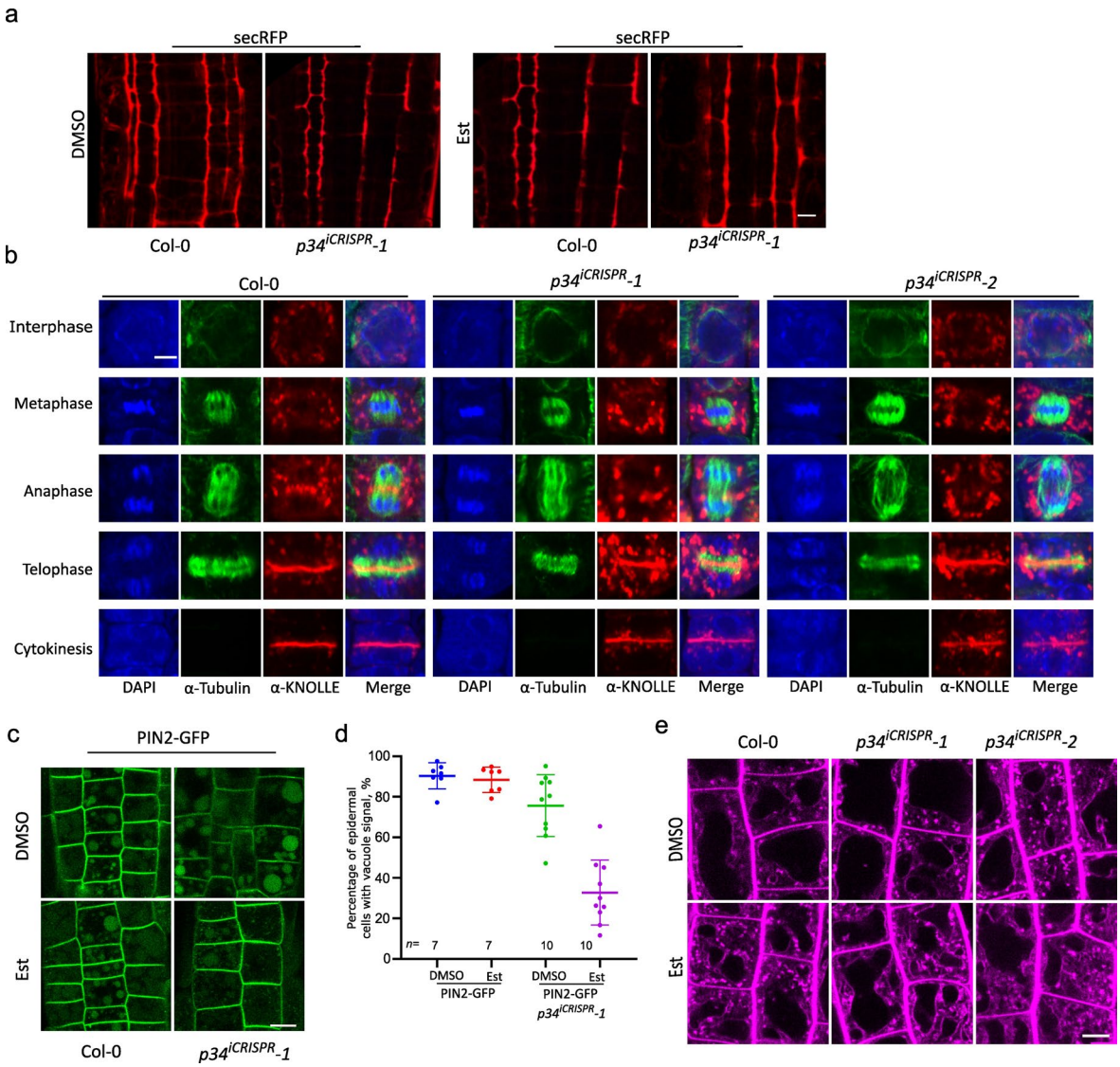

Extended Data Fig. 10 | Vesicular trafficking pathways affected in the *p34* mutants. a, secRFP localization in roots of 5-day-old Col-0 and *p34*^{iCRISPR}*-1* plants grown on DMSO and 10 μM β-oestradiol (Est). **b**, Immunofluorescence staining of KNOLLE in the root meristem of Col-0, *p34*^{iCRISPR}*-1* and *p34*^{iCRISPR}*-2* plants treated with 10 μM Est. **c**, PIN2-GFP localization in the roots of 5-day-old Col-0 and *p34*^{iCRISPR}*-1* plants grown on DMSO and 10 μM Est in the dark. **d**, Percentage of epidermal cells with GFP signals in the vacuoles as shown in (**c**), Error bars represent SD. **e**, Morphology of the lytic vacuoles in root cells of 7-day-old Col-0, *p34*^{iCRISPR}*-1* and *p34*^{iCRISPR}*-2* plants grown on DMSO and 10 μM Est. Images were taken after 2 h of staining with 4 μM FM4-64. Scale bars, 10 μm (**a-c**,**e**), The imaging of all genotypes was repeated three times. One representative experiment is shown.

nature portfolio

Corresponding author(s): Wei Siao
Eugenia Russinova

Last updated by author(s): Nov 22, 2022

Reporting Summary

Nature Portfolio wishes to improve the reproducibility of the work that we publish. This form provides structure for consistency and transparency in reporting. For further information on Nature Portfolio policies, see our Editorial Policies and the Editorial Policy Checklist.

Statistics

For all statistical analyses, confirm that the following items are present in the figure legend, table legend, main text, or Methods section.

n/a	Confirmed	
☐	☒	The exact sample size (*n*) for each experimental group/condition, given as a discrete number and unit of measurement
☐	☒	A statement on whether measurements were taken from distinct samples or whether the same sample was measured repeatedly
☐	☒	The statistical test(s) used AND whether they are one- or two-sided *Only common tests should be described solely by name; describe more complex techniques in the Methods section.*
☐	☒	A description of all covariates tested
☐	☒	A description of any assumptions or corrections, such as tests of normality and adjustment for multiple comparisons
☐	☒	A full description of the statistical parameters including central tendency (e.g. means) or other basic estimates (e.g. regression coefficient) AND variation (e.g. standard deviation) or associated estimates of uncertainty (e.g. confidence intervals)
☐	☒	For null hypothesis testing, the test statistic (e.g. *F*, *t*, *r*) with confidence intervals, effect sizes, degrees of freedom and *P* value noted *Give P values as exact values whenever suitable.*
☒	☐	For Bayesian analysis, information on the choice of priors and Markov chain Monte Carlo settings
☒	☐	For hierarchical and complex designs, identification of the appropriate level for tests and full reporting of outcomes
☒	☐	Estimates of effect sizes (e.g. Cohen's *d*, Pearson's *r*), indicating how they were calculated

Our web collection on statistics for biologists contains articles on many of the points above.

Software and code

Policy information about availability of computer code

Data collection	-For AP-MS, stoichiometric analyses and Proximity Labeling, proteins were identified with either Mascot Distiller software (version 2.5.0.0; Matrix Science) combined with the Mascot search engine (versions 2.5.1 and 2.6.2; Matrix Science) using the Mascot Daemon interface or with MaxQuant (version 1.6.10.43). -For confocal image collection: Las-X software (v 3.5.0.18371) for Leica SP8 confocal microscope; Zen 2009 for Zeiss 710 confocal microscope; Olympus FV10-ASW for Olympus FluoView confocal microscope. -For DIC image collection: Olympus BX51. -For immunoblotting: Image Lab Software 3.0 (Bio-RAD). -For the guide RNA design: Online tool CCTOP(https://cctop.cos.uni-heidelberg.de:8043/)
Data analysis	- For AP-MS and Proximity Labeling, NSAF values were analyzed with the KNIME Analytics Platform (versions 4.0.2 en 4.4.0). For Proximity Labeling, LFQ intensities were analyzed in Perseus, version 1.6.15.0. The integrative modeling platform (IMP) package (version 2.12) was used for structural analysis. - For PL-MS, raw MS data was analyzed with pLINK2 version 2.3.5. - For Sequences aligned : Qiagen CLC Main Workbench 8.1 - For imaging data analysis: ImageJ(ImageJ1.53t) and FIJI (https://imagej.nih.gov/ij/) - For statistical data analysis: GraphPad Prism 8.0 (https://www.graphpad.com/) -For the CRISPR analysis: online ICE Analysis Tool v3.0(https://ice.synthego.com/) -For immunoblotting analysis: Image Lab Software 3.0 (Bio-RAD).

For manuscripts utilizing custom algorithms or software that are central to the research but not yet described in published literature, software must be made available to editors and reviewers. We strongly encourage code deposition in a community repository (e.g. GitHub). See the Nature Portfolio guidelines for submitting code & software for further information.

Data

Policy information about availability of data

All manuscripts must include a data availability statement. This statement should provide the following information, where applicable:

- Accession codes, unique identifiers, or web links for publicly available datasets
- A description of any restrictions on data availability
- For clinical datasets or third party data, please ensure that the statement adheres to our policy

The mass spectrometry proteomics data have been deposited to the ProteomeXchange Consortium via the PRIDE partner repository with the dataset identifier PXD035454 and 10.6019/PXD035454.

Human research participants

Policy information about studies involving human research participants and Sex and Gender in Research.

Reporting on sex and gender	n/a
Population characteristics	n/a
Recruitment	n/a
Ethics oversight	n/a

Note that full information on the approval of the study protocol must also be provided in the manuscript.

Field-specific reporting

Please select the one below that is the best fit for your research. If you are not sure, read the appropriate sections before making your selection.

☒ Life sciences ☐ Behavioural & social sciences ☐ Ecological, evolutionary & environmental sciences

For a reference copy of the document with all sections, see nature.com/documents/nr-reporting-summary-flat.pdf

Life sciences study design

All studies must disclose on these points even when the disclosure is negative.

Sample size	Sample size was determined based on empirical knowledge and publications with similar content. For quantification of root-related phenotype, about 20 roots for each experiment were measured. For quantification of leaf area, about 8 plants for each experiment were measured. For quantification of embryo phenotype, about 50 embryos from 3 siliques for each experiment were measured. For rBiFC experiments, at least 10 cells for each experiment were measured. For quantification of PM/Cyto fluorescence intensity, about 4 cells for each root and about 8 roots for each experiments were quantified. For quantification of protein levels, 3 bands were quantified.
Data exclusions	No data was excluded
Replication	All experiments were repeated 2 or 3 times with similar outcomes.
Randomization	In experiments involving multiple genotypes, seedlings were grown on multiple plates at different positions randomly on the racks. For experiments with chemical treatments, we grew seedling for different treatments on separate plates that were always placed randomly on the racks in the same parts of the growth chamber to minimize variations in growth conditions.
Blinding	Blinding was not applied. All the quantification analyses were done with the same criteria and the same software as described in the Methods to ensure unbiased quantification. Our study is to provide resources by building a comprehensive protein interaction network of AP complexes. The interactome results are based on the purification steps and the filtering parameters. For the functional study of P34, we didn't proposed any preferred model but just to show which pathways and which proteins are or are not affected.

Reporting for specific materials, systems and methods

We require information from authors about some types of materials, experimental systems and methods used in many studies. Here, indicate whether each material, system or method listed is relevant to your study. If you are not sure if a list item applies to your research, read the appropriate section before selecting a response.

Materials & experimental systems

n/a	Involved in the study
☐	☒ Antibodies
☐	☒ Eukaryotic cell lines
☒	☐ Palaeontology and archaeology
☒	☐ Animals and other organisms
☒	☐ Clinical data
☒	☐ Dual use research of concern

Methods

n/a	Involved in the study
☒	☐ ChIP-seq
☒	☐ Flow cytometry
☒	☐ MRI-based neuroimaging

Antibodies

Antibodies used

-Commercial antibodies:
anti-GFP (Miltenyi Biotec, catalog :130-091-833,clone name: GG4-2C2.12.10, lot: 5220806418)
anti-RFP (ChromoTek, anti-RFP antibody,Clone name: 6G6 , lot: 51020014AB-04),
anti-tubulin (Sigma-Aldrich, T5168, clone name: B-5-1-2, monoclonal, lot: 039M4769V),
anti-CHC (Santa Cruz, catalog : sc-57684, lot:#C0311),
ECL Rabbit IgG, HRP-linked whole Ab (from donkey) (Amersham, Cat. No. NA934V-1ML, Lot. No. 17624274)
ECL Mouse IgG, HRP-linked whole Ab (from sheep) (Amersham, Cat. No. NXA931V-1ML, Lot. No. 17457723)
AlexaFluor488 goat anti-mouse (A-11001, Thermo Fisher Scientific),
AlexaFluor555 donkey anti-rabbit (A-31572, Thermo Fisher Scientific),

-othre antibodies
anti-PIN2 (Abas, Lindy, et al. 2006, gift from Dr Christian Luschnig, Institute for Applied Genetics and Cell Biology, University of Natural Resources and Applied Life Sciences, Austria),
anti-AP2S (Wang, C. et al. 2016, gift from Prof. Jianwei Pan, Yan Xu , Lanzhou University, China),
anti-AP2A (Song, K. et al. 2012, gift from Prof. Inhwan Hwang, Pohang University of Science and Technology, Korea)
anti-AP1G (Kim, Y. W. et al. 2001, gift from Prof. Inhwan Hwang, Pohang University of Science and Technology, Korea),
anti-TPLATE (Dejonghe, Wim, et al. 2019, TPLATE antibody custom made by Biotem in rabbits previously, Ugent-PSB),
anti-KNOLLE (Lauber, Martina H., et al. gift from Dr. Gerd Jürgens, Max-Planck-Institut für Entwicklungsbiologie, Germany)

Validation

anti-GFP (specifically reconizes wild-type GFP from Aequorea victoria and derivatives, e.g., EGFP, CFP, YFP, and BFP.),
anti-RFP (Tested on mRFP, mCherry, mPlum, mOrange, mRFPruby, DsRed, mScarlet, mScarlet-I, OFP, tdTomato.),
anti-CHC (raised against sucrose purified clathrin coated vesicles of soybean origin.)
anti-tubulin (Recognizes an epitope located at the C-terminal end of the α-tubulin isoform in a variety of organisms.)
anti-PIN2 (immunoprecipitations membrane protein (up to 100 µg) was solubilized in RIPA buffer with protease inhibitors and incubated overnight with affinitypurified rabbit anti-PIN2)
anti-AP2S (antibody were raised in rabbits using synthesized peptides, validated in total protein extracts from leaf tissues.)
anti-AP2A (western-blot analyses were performed with the anti-a-adaptin antibody using protein extracts from protoplasts transformed with HA:a-adaptin.)
anti-AP1G (MBP:γ-adaptin was used to immunize rabbits and antibody was affinity-purified using recombinant proteins.To confirm the specificity of the anti–γ-adaptin antibody, protein extracts from protoplasts transformed with HA:γ-adaptin were used in Western blot analysis)
Anti-TPLATE (TPLATE antibody was generated in New Zealand White rabbits (BIOTEM, France); Reactivity: Arabidopsis thaliana; Application: WB; Validated-in house via western blotting with comparative analysis of complemented mutant plants LAT52:TPLATE-GFP/tplate (-/-) and Col-0 using an anti-GFP and the anti-TPLATE antibody)
anti-KNOLLE (The antibody was purified by affinity chromatography with purified KN protein coupled to cyanbromide-activated Sepharose and elution of bound antibodies with 2.5 M and 4 M MgCl2. Purified antibody gave the same signals as the whole antiserum in immunolocalization experiments.)

Eukaryotic cell lines

Policy information about cell lines and Sex and Gender in Research

Cell line source(s)	The PSB-D wild-type cell line is available at the ABRC with stock number CCL84840. https://abrc.osu.edu/stocks/282
Authentication	The cell lines were not authenticated.
Mycoplasma contamination	The cell lines were not tested for mycoplasma contamination.
Commonly misidentified lines (See ICLAC register)	No commonly misidentified cell lines were used in the study